Ternary Thiophene-X-Thiophene Semiconductor Building Blocks (X= Fluorene, Carbazole, Phenothiazine): modulating electronic properties and electropolymerization ability by tuning the X core

Alessandra Tacca[a]*, Riccardo Po[a], Maria Caldararo[a], Stefano Chiaberge[a], Liliana Gila[a], Luca Longo[a], Patrizia Romana Mussini[b,1], Andrea Pellegrino[a], Nicola Perin[a], Mario Salvalaggio[a], Alberto Savoini[a], Silvia Spera[a]

[a]Centro Ricerche per le Energie non Convenzionali, Istituto ENI Donegani, ENI S.p.A., Via G. Fauser 4, 28100 Novara, Italy

[b]Dipartimento di Chimica Fisica ed Elettrochimica, Università degli Studi di Milano, Via Golgi 19, 20133 Milano, Italy

[1]ISE Member.

* Corresponding author, Tel.: +39 0321 447411; fax: +39 0321 447425, E-mail address: alessandra.tacca@eni.com.

Abstract

To achieve rationalization criteria for target-oriented molecular design of Th-X-Th (Th = thiophene) semiconductor building blocks, we have carried out an extensive investigation on the effects of the X core (X = fluorene, carbazole or phenothiazine) on the electronic properties and polymerization ability of Th-X-Th monomers and on the electronic and structural properties of the corresponding periodic conducting polymers -(Th-X-Th)$_n$-, obtained by electropolymerization and, for comparison's sake, by $FeCl_3$-catalyzed polymerization and/or Suzuki coupling. The effects of molecule bending and of solubilising bulky alkyl substituents have also been considered. The systematic, exhaustive template sequence combined with a rigorous, multitechnique investigation protocol affords a unique data library and a complete set of reliable interpretative/predictive guidelines

Keywords

Molecular electronics

Semiconductor building blocks

Electropolymerization

Conducting polymers

HOMO–LUMO tuning

1. Introduction

Conjugated polymeric systems based on thiophene, carbazole or fluorene are among the most promising materials for the development of new generation, highly efficient organic photovoltaic devices [1-3]. These monomer units, especially in combination with electron-poor aromatic units, lead to novel polymeric electron donor structures [4-8] that possess a number of properties useful for increasing the photovoltaic response [2], such as an energy level alignment with electron acceptors [9]; a low energy gap which favours the light harvesting and increase the short-circuit current of the device [4]; a fair hole mobility [10] and good solubility in organic solvents and film forming characteristics [11].

Alternating copolymers of fluorene, thiophene and benzothiadiazole or benzopyrazine (APFOs) have been widely studied by Inganäs *et al.* [12-18]. The fluorene unit imparts to the material a fairly good stability and a high mobility. The gaps of the copolymers are reduced and tuned by the introduction of electron-poor units [19-28]. The 2,7-substitution prevents the formation of kinked structures and maintains a good linearity of the polymer chain. The linking between fluorene units (6-membered rings) and thiophene units (5-membered rings) contributes to mitigate any steric distortion, to keep the structure planar and to increase the conjugation. Polymer solar cells based on APFO polymers have power conversion efficiencies in the range 0.6-4%.

Leclerc et al. [29-31] developed a class of polymer donors based on carbazole, thiophene and several electron-poor units (including benzothiadiazole) which afforded solar cells with efficiencies as high as 6.1% [32]. The polymer structurally similar to poly{9,9-bisalkylfluorene-2,7-diyl-*alt*-[4,7-bis(thien-2-yl)-2,1,3-benzothiadiazole]-5'-5"-diyl}, where the fluorene unit is substituted by a 2,7-carbazole unit, exhibits comparable optoelectronic characteristics but an improved hole mobility. In general, copolymers of 2,7-carbazole have better optical properties than 3,6-carbazole copolymers [33].

Another heterocyclic unit recently reported, promising for photovoltaic applications and structurally related to 3,6-carbazole, differing for the introduction of a sulphur atom bridging the two phenylene moieties, is phenothiazine [34].

Optimized molecular design of target-oriented materials in the above multivariate, virtually unlimited field urgently requires that reliable rationalization criteria be made available concerning relationships among molecular structure, electronic properties and polymerization ability. This can only be achieved by performing ponderous multidisciplinary studies on systematic molecular series, which is too often overlooked in favour of specific applicative developments.

Aiming to contribute to fill this gap, we have carried out the present extensive investigation, focused on the effects of a non-thiophene central conjugated system X (X = fluorene ["Fluo"], carbazole ["Cbz"], or phenothiazine ["Phen"]) on the electronic properties and polymerization ability of Th-X-Th monomers (Th = thiophene), and on the electronic and structural properties of the corresponding periodic conducting polymers -(Th-X-Th)$_n$-, obtained by electropolymerization and, for comparison's sake, by $FeCl_3$ oxidative polymerization and/or Suzuki coupling.

A synopsis of the investigated molecules is provided in Figure 1. In particular, we have focused on the following three templates:

2,7 Th-Fluo-Th (represented by monomer **F_1**)

2,7 Th-Cbz-Th (represented by monomers **C_1**, **C_2**)

3,7 Th-Phen-Th (represented by monomers **P_1**, **P_2**, **P_3**)

in which the thiophene side units are linked to the central conjugated system (Fluo, Cbz, or Phen) in the positions granting the highest linearity and, therefore, conjugation efficiency (*i.e.* the 2,7 ones in the Fluo and Cbz cases and the 3,7 one in the Phen case).

We have, however, also considered the effect of changing the positions of the thiophene units by including in our study the following template:

3,6 Th-Cbz-Th (represented by monomers $\mathbf{C'_1}$, $\mathbf{C'_2}$)

implying a kinked structure.

(Figure 1 here)

As it is shown in Figure 1, in all our monomers the core ring is substituted with a bulky alkyl chain, either linear ($\mathbf{P_1}$, $\mathbf{C'_1}$) or branched ($\mathbf{F_1}$, $\mathbf{C_1}$, $\mathbf{C_2}$, $\mathbf{P_2}$, $\mathbf{P_3}$, $\mathbf{C'_2}$), affording high solubility in the most widespread organic solvents.

Finally, a comparison between a -(Th-X-Th)$_n$- periodic polymer and the corresponding -(Th-X)$_n$- one has also been achieved by applying the Suzuki coupling approach to Th-Fluo-Th monomer $\mathbf{F_1}$ and to the corresponding Th-Fluo one $\boldsymbol{f_1}$.

2. Experimental

2.1. Synthesis

All the monomers and polymers have been synthesized through Suzuki reaction [35], with tetrakis(triphenylphosphine)palladium(0) as catalyst. For sake of comparison, some polymers were prepared by chemical oxidation route with iron trichloride [36].

Appendix A provides a general synthetic scheme, together with full details concerning the specific syntheses of each monomer, monomer precursor, and chemically synthesized polymer.

2.2. DFT Calculations

The molecular models described in this study were obtained by Density Functional Theory optimization [37-42]. The chosen software was Amsterdam Density Functional (ADF) from SCM [43] and the computing platform was our High Power Scientific Computing system (180 AMD Opteron and AMD Athlon based parallel processing units, Linux RH Enterprise ed.operative system, with 580 GB of RAM and 6TB of mass storage).

The basis functions adopted for all those models are TZP Slater Type Orbitals [44-47].

The DFT calculations are performed with the Vosko-Wilk-Nusair local density approximation (LDA) [48] combined with two Generalized Gradient Approximations (GGA): the method in which the BP-86 exchange functional proposed by Becke is combined with the correlation functional developed by Perdew [49-51], and the hybrid method B3-LYP [37, 52]. The parameterizations employed and the convergence criteria adopted are listed in Appendix B.

For each model, the frontier orbitals HOMO and LUMO have been plotted in Figure 2. The excitation analysis had been performed by means of Time Dependent Density Functional Theory (TD-DFT) [53-55]; calculations were carried out based on geometries optimized by means ADF with the previously described method. For each excitation, the composition of the solution vector of the TD-DFT eigenvalue problem from which the transition dipole moments are computed [56-58] in terms of contributions from pairs of occupied and virtual MOs allows a convenient and intuitive analysis of the results in terms of “excitations” from occupied to virtual Kohn-Sham orbitals [59].

We applied the Davidson iterative procedure for the computation of the eigenvalues and the eigenvectors of the TDDFT equation [60].The parameterizations adopted in the excitation analysis and in the theoretical prediction of the UV/Vis spectra are listed in Appendix B.

2.3. Spectroscopy

UV-Vis: absorption spectra were recorded at room temperature with a Perkin-Elmer Lambda 950 spectrophotometer. Samples in solution were prepared by dissolving monomers in CH_3CN or CH_2Cl_2 solutions in cell with 10 mm optical path length and optical density of typically 0.5 at max. absorption in the visible region of spectrum. The optical energy gaps were evaluated by the edge corresponding to the intersection between the negative tangent line in the inflection point of lowest energy absorption band and the tangent line to linear portion of the absorption tail.

Steady-state PL: photoluminescence spectra were recorded at room temperature with a Horiba Jobin-Yvon Fluorolog 3 spectrofluorometer, with right angle geometry. The excitation wavelength Quantum Yield measurements were recorded at room temperature with the integrating sphere F-3018 by Horiba Jobin-Yvon on Fluorolog 3, for absolute luminescence determination.

Time-Resolved PL: photoluminescence decays were obtained with TCSPC apparatus from Horiba Jobin-Yvon on Fluorolog 3; light excitations were provided by nanoled (1ns FWHM) at 309nm for **C'$_1$** and by nanoledL (200ps FWHM) at 378 nm for **F$_1$**, **C$_1$**, **P$_3$**.

2.4. Electrochemistry

The cyclovoltammetric (CV) characterization was carried out using an Autolab PGSTAT 12 potentiostat/galvanostat (EcoChemie, The Netherlands) run by a PC with GPES software. The monomer solutions were 0.0002-0.0004 M in acetonitrile solvent (Carlo Erba, HPLC grade) with 0.1 M tetrabutylammonium tetrafluoroborate TBATFB (Fluka, electrochemical grade) as supporting electrolyte, and were deareated with nitrogen purging. The working cell included a Glassy Carbon GC disk embedded in Teflon® (Amel, surface 0.071 cm^2) as the working electrode, the polishing procedure consisting in surface treatment with alumina powder (Metrohm) on wet filter paper; a Platinum counter electrode (Metrohm); and an aqueous saturated calomel electrode

(SCE, Amel) as the reference electrode. According to IUPAC recommendations the data have been referred to the Fc^+/Fc redox couple (ferricinium/ferrocene), having a formal potential of 0.390 V *vs* our operating reference electrode [61]. The ohmic potential drop was compensated by the positive feedback technique [62].

Polymers were electrosynthesized from the same solutions, on the same GC electrode and on ITO electrodes (Indium Tin Oxide, Aldrich, average operating surface 2 cm^2, sheet resistance 15-25 Ω/sq), cycling the potential around the first oxidation peak corresponding to carbocation formation (typical range: 0.5-1.2 V (SCE)), at 0.2 V s^{-1} scan rate, for 48 cycles. The CV stability of the films was tested by repeated cycling in the same potential range, in monomer-free ACN solutions with 0.1 M TBATFB supporting electrolyte; finally, the potential range was progressively extended negatively in search for the first reduction potential and possible related charge-trapping phenomena.

Polymers synthesized by Suzuki coupling or by oxidative polymerization with $FeCl_3$ were dissolved in chloroform (1 mg cm^{-3}); the solution was drop-coated on the GC electrode from a calibrated capillary, after which the same above characterization in monomer-free solution was repeated following the same protocol as for the electrosynthesized films. In this case, however, observation of reproducible redox behaviour with full exploitation of the redox active sites required in most cases a preconditioning step consisting in repeated potential cycling in a suitable range, in which the polymer network could give off residuals of chemicals from the synthetic step and become fully conditioned in the new medium.

2.5. AFM microscopy

The nanoscale morphologies of the polymers were studied using tapping-mode Atomic Force Microscopy AFM (Multimode IIID microscope, Veeco).

Surface topography and phase images were taken in air and at room temperature.

3. Results and Discussion

3.1. Theoretical modelling

The quantum mechanical models object of this paper can be formally considered as Thiophene-X-Thiophene (Th-X-Th) trimers, where X can be Fluorene (Fluo) or Carbazole (Cbz) or Phenothiazine (Phen). In particular, six different templates have been considered, in which the thiophene rings are always *alpha* bonded while the central X units are bonded to them either in 2,7 (3,7 in the Phen case) or in 3,6 positions. Whenever heteroatom positions able to carry alkyl substituents are present, they have been assumed to be simply saturated with methyl groups.

A highlight of the computational results is provided by Tables 1 and 2 and Figure 2.

(Figure 2 here)

From a structural point of view, the most remarkable differences within the molecules under investigation arise from the differences in the bond angles of the central unit. 2,7 Th-Fluo-Th and 2,7 Th-Cbz-Th are almost superimposable and show no significant differences in bond geometries apart from the quaternary C-aromatic C bond in Th-Fluo-Th being 1.53 Å while the N-aromatic C only 1.39 Å. This results in a distortion in the 5-membered aromatic ring, which slightly increases the Th-X-Th angle in the Cbz-based system with respect to the analogous Fluo- one. The structure of 3,7 Th-Phen-Th is a peculiar case because the central 6-membered heterocyclic ring is strongly folded. While the two systems previously analyzed are almost flat and, if we neglect the methyl substituents and the slight tilt of the σ bonds, could both belong to the C_{2V} Abelian Point Group, the 3,7 Th-Phen-Th system shows an angle of 144° between the two molecular planes that intersect along the N and S atoms and definitively belongs to the C_s Point Group only. If compared with the previously analyzed two systems, the angle between the central unit and the two thiophene substituents is strongly distorted from planarity (Figures 2 and Figure B1 in Appendix B).

The Th-Cbz-Th geometry is strongly influenced by the two possible bonding positions for the thiophene units (Figures 2 and B1). The 2,7 bonding results in a 155° angle between the two

thiophene-core σ bonds, while the 3,6 bonding bears an angle of -89°, the minus sign accounting for the angle being on the opposite side of the molecule with respect to the core N taken as the reference. This feature must influence the geometry of a polymer composed by these triplets and the packing of the resulting systems. Moreover it is worthwhile noticing that in 3,6 model the thiophene S atoms appear to be more stable in σ trans conformation with respect to the core N, while they result σ cis in the 2,7 model.

(Table 1 here)

(Table 2 here)

From an electronic point of view, all systems feature dihedral angles along thiophene-core σ bonds which are almost, but never completely, flat [63]. The rather small distortions from planarity, *i.e.* 22° for Th-Flu-Th, 27° for Th-Cbz-Th and 24° for Th-Phen-Th, account for slightly different balances between a prevailing effect of the additional stabilization energy associated with hyperconjugation, fostering planarity, and a weaker effect of sterical hindrance, which in itself would push the bonds towards right angles. In particular, the above angles point to the Th-Flu-Th system affording the highest M.O. superimposition (and energy stabilization) in the series. This can be due to the absence of polarization arising from the presence of heteroatoms in the neighbourhood of the bond.

The electronic distribution of the systems under investigation is strongly influenced by the presence of heteroatoms along the aromatic rings. In fact, the Th-Phen-Th shows the higher dipole moment (see Table 5) immediately followed by Th-Cbz-Th; the model Th-Fluo-Th, bearing a pure alkene polycyclic core, shows the lower molecular dipole moment, produced almost entirely by the polarization of the thiophene units.

Analysis of the frontier orbital distribution (Figure 2) shows that, in every case, the corresponding M.O. are on the hyperconjugated π system and bear a nodal plane on the σ bond frame. While the HOMO is extended almost evenly on the whole system in both the Th-Fluo-Th and Th-Cbz-Th

molecules, in Th-Phen-Th it is concentrated on the core fragment. Instead in the C' case in spite of the kinked structure the HOMO orbital appears to be distributed along the whole molecule; thus conjugation between the two side thiophene units appears to be hampered but not completely lost. This is in agreement with experimental evidence (Paragraphs 3.2 and 3.3).

It is worthwhile mentioning that the quaternary C in Fluo, N in Cbz and N and S in Phen do not directly contribute to any of the frontier orbitals, which are exclusively localized on the carbon scaffolds of all the examined systems.

The theoretical excitation analysis was performed in order to allow prediction of the UV/Vis spectra, as reported in the experimental section. The obtained results have been used to understand the origin of the single peaks forming the UV-Vis absorption spectra (see paragraph 3.2): the excitation energies and oscillator strengths of the most relevant transitions are available in Appendix B.

3.2. UV-Vis Spectroscopy

UV-visible absorption and emission spectra of **F_1**, **C_1**, **C'_1**, **P_3**, representing our four monomer templates, are reported in Figure 3. All of them have been recorded in CH_3CN (ACN) solution and have been normalized on the lowest-energy absorption band; in particular, the absorption spectrum of **P_3** has been normalized at 353 nm. HOMO-LUMO optical energy gaps have been calculated from the onset of the lowest energy absorbance peak, as detailed in the experimental section; they correspond to the minimum amount of energy which will promote the electronic transition from ground to excited state. Another highly significant parameter, useful in the following discussion, is the energy matching the most probable electronic transition as determined from the maxima of the lowest-energy absorption band. Such data are collected in Table 3 together with the corresponding electrochemical data (described in the following paragraph 3.3), for all monomers and for both the operating solvents.

(Figure 3 here)

(Table 3 here)

F$_1$ exhibits a main absorption envelope in the near-UV region with maximum at 351 nm and a lower intensity band centred at 243 nm. In particular, on the basis of the theoretical calculations, the 351 nm band can be attributed to the HOMO-LUMO π–π* transition which involves the all-C scaffold, with a nearly complete exclusion of the sp^3 carbon of the fluorene unit (Figure 2). The 243 nm band has a π–π* character and the transition is nearly exclusively localized into the thienyl units. (For more details, see Appendix B). Moreover, F_1 presents a strong structured fluorescence emission with a small Stokes shift (3500 cm^{-1}), suggesting a rather rigid, highly planar conjugated system both in ground and excited states; the more finely structured emission pattern, however, points to the ground state being even more rigid than the excited one.

C$_1$ features two main absorption structured bands in the near-UV region, with maxima at 270 and 350 nm, respectively. Again the theoretical computations provide valuable clues for their assignment. In particular, while the 270 nm band (attributable to a π–π* transition localized within the carbazole core unit) is a peculiar feature of this monomer, the 350 nm structured absorption is nearly coincident with the main band observed for **F$_1$** monomer. This is due to the fact that these π–π* transitions involve the same portion of backbone conjugated moiety and the electron densities of the HOMO and LUMO are very similar for these monomer templates. Consequently, C_1 presents a similar strong structured fluorescence emission with a slightly higher Stokes shift (4040 cm^{-1}) than **F$_1$**.

In the case of kinked **C'$_1$** the absorption peak corresponding to the lowest energy (attributable, again, to a π–π* transition between molecular orbitals delocalized on the entire molecule) is shifted to 313 nm, while the emission peak nearly coincides with the **C$_1$** one.

Both features can be justified on the basis of very similar potential energy curves of their ground states and different potential energy curves of their lowest excited states, but with the same minimum for both **C$_1$** and **C'$_1$**; on the basis of this assumption, the curve representing the lowest excited state should have a stronger harmonic oscillator constant (*k*) in the **C'$_1$** case, leading to a

Franck-Condon state at higher energy. This hypothesis of stronger *k* for **C'$_1$** with respect to **C$_1$** is supported by the theoretical calculations suggesting a **C'$_1$** LUMO orbital less delocalized than in **C$_1$**.

As gathered from the corresponding HOMO and LUMO depicted in Figure 2, the greater vibrational freedom of the thienyl units in **C'$_1$** with respect to **C$_1$** favours non-radiative decay pathways, as confirmed by the corresponding lower Quantum Yield QY data (Table 4).

(Table 4 here)

P$_3$ shows a very different pattern with three absorption bands at 240, 288, and 354 nm. In particular, the lowest-energy broad absorption is attributable to the HOMO-LUMO $\pi-\pi*$ transition which involves an electronical density redistribution from the central core mojety towards the peripheral thienyl units (Figure 2), followed by a change in nuclear coordinates from a partially bent structure (24° dihedral angles between Th-Phen-Th units, as obtained by theoretical modelling) to a more planar geometry [64], with the consequent largest Stokes shift (7500 cm^{-1}) in the series. Otherwise, the sharp and intense 288 nm band involves redistribution from the conjugated backbone comprising the central core sulphur atom to the thienyl, with a minor change in nuclear configuration (Appendix B).

All spectra have also been measured in CH_2Cl_2 solution, displaying no significant medium effect (Table 3).

Moreover, the absorption spectra of 2,7 Th-Cbz-Th significantly depend on the monomer concentration, suggesting aggregation phenomena [65].

QY measurements show the highest value for **F$_1$** monomer, characterised by a rigid highly planar structure; consistently, systems like fluorene are widely used as emitters for OLED applications [66, 67]. Excited state **C$_1$** structure is very similar to **F$_1$** (Figure 3), but the QY is about the half, probably due to the presence of heteroatom; **C'$_1$** shows a QY about one tenth of **C$_1$** one because the LUMO state is not completely rigid, and the thienyl units are free to rotate, thus increasing the non-radiative decay constant (k_{nr}) (*vide supra*).

All lifetimes are in the order of few nanoseconds; $\mathbf{F_1}$ has the lowest value due to a highly efficient radiative decay, instead $\mathbf{C_1}$ shows the longest lifetime suggesting more exciton delocalization, but has a lower k_r.

3.3 Electrochemistry

3.3.1 Electrochemistry of the monomers.

The eight monomers $\mathbf{F_1}$, $\mathbf{C_1}$, $\mathbf{C_2}$, $\mathbf{C'_1}$, $\mathbf{C'_2}$, $\mathbf{P_1}$, $\mathbf{P_2}$, $\mathbf{P_3}$ have been studied by cyclic voltammetry (CV) in acetonitrile; a synopsis of CV characteristics at 0.2 V s^{-1} scan rate is reported in Figure 4, each of them assembled as a combination of an anodic and a cathodic half-cycle, in order to exclude any signal distortion as a consequence of electrode fouling by products of chemical steps following the electron transfer ones.

(Figure 4 here)

First oxidation peaks.

For the three templates 2,7 Th-Fluo-Th, 2,7 Th-Cbz-Th, and 3,6 Th-Cbz-Th, the first oxidation peaks are consistent with a chemically irreversible electron transfer (no symmetric return peak, trace of deposition of an electrochemically active, reducible layer on the electrode surface), pointing to the tested molecules being able to undergo oligomerization upon potential cycling around the first oxidation peak. It is worthwhile noticing that such electrochemical oligomerization must take place on the only two available α-thiophene positions, *i.e.* the terminal, symmetrical ones in the template, thus resulting in the formation of regioregular –(Th-Fluo-Th)$_n$- or –(Th-Cbz-Th)$_n$- oligomers, which can be also regarded as –(Th-Th-Fluo)$_n$- or –(Th-Th-Cbz)$_n$-, featuring bithiophene units alternating with Fluo or Cbz ones. This is also consistent with the theoretical computations, pointing to the HOMO orbital significantly involving the peripheral thiophene rings, albeit not exclusively. The first oxidation peak potentials are more positive for the 2,7 Th-Fluo-Th template than for the 2,7 Th-Cbz-Th ones, which is consistent with the presence of the heteroatom in the latter cases, making them electron richer. An even larger difference is observed between 2,7 Th-

Cbz-Th and 3,6 Th-Cbz-Th, *i.e.* the change in the molecular geometry from linear to angular appears to have a higher impact than the presence of the nitrogen atom.

The case of template 3,7 Th-Phen-Th is remarkably different; not only the first oxidation peaks are the least positive in the series, but the CV oxidation pattern features two neatly separated chemically and electrochemically reversible oxidation peaks, accounting for the subsequent formation of a stable radical cation (first electron transfer) and dication (second electron transfer), with no tendency to oligomerization. The low oxidation potentials point to the phenothiazine core affording the electron richest template in the sequence, while the stability of the positively charged products could be justified assuming that the high local electron density of the phenothiazine core (originating from the presence of the two heteroatoms) results in both stabilization of the positive charge and its localization within the phenothiazine core, which of course would totally hamper oligomerization. This is consistent with theoretical computations (see paragraph 3.1) pointing to the HOMO being localized on the phenothiazine core, unlike the LUMO.

It is worthwhile noticing that, normalized current densities having been reported in Figure 4, in all irreversible cases the first oxidation peaks appear significantly higher than the reversible ones. This is consistent with an EC mechanism (electron transfer followed by chemical reaction), resulting in a higher peak with respect to a E_{rev} (reversible monoelectronic electron transfer) case [68], including the particular cases of oligomerization [69] and polymerization [70]. Therefore the above feature does not necessarily point to the two terminal thiophene positions being independent and, as a consequence, equivalent, which would result, of course, in a monoelectronic peak of double height. Actually the latter assumption seems more appropriate for a significantly kinked template like C', while it appears less likely for the nearly planar systems where the two terminal positions would be still too close and the conjugation too effective, since no nodes can be reasonably assumed to be present along the chain, according to a criterion recently proposed by some of us [71].

First reduction peaks.

The first reduction peaks appear at very negative potentials (consistently with the low electron acceptor character of all our templates) providing the onset of some complex irreversible process; this makes their morphological analysis quite difficult. We can only observe that they are very similar in shape and chemically irreversible for all templates; however they exhibit a significant shift to more negative potentials in the template sequence 2,7 Th-Fluo-Th , 2,7 Th-Cbz-Th , 3,6 Th-Cbz-Th, 3,7 Th-Phen-Th, thus corresponding to increasingly electron richer systems, in agreement with the above discussed anodic potential series. Actually, it is a well known feature that whenever the first oxidation and first reduction site coincide, inductive effects should result in rigid translation of the CV pattern towards more negative potentials (easier oxidation, more difficult reduction) upon introduction of electron donating substituents, or towards more positive potentials (more difficult oxidation, easier reduction) upon introduction of electron attracting substituents. The fact that in our case translation is not rigid (and the distance between first oxidation and reduction peak not constant) points to the incipient radical cation and anion being differently delocalized on the conjugated system.

Electrochemical HOMO and LUMO levels and gaps.

From the first oxidation and reduction peak potentials, values of HOMO and LUMO levels can be estimated by the following equations [72, 73] ultimately based on the absolute value for the normal hydrogen electrode (NHE) critically assessed in a fundamental review paper: [74]

$$E_{HOMO}\ (\text{eV}) \approx -1\text{e} \times [\ (E_{p,a}\ (\text{V } \textit{vs}\ \text{Fc}^{+}|\text{Fc}) + 4.8\ (\text{V Fc}^{+}|\text{Fc vs zero})] \qquad (1)$$

$$E_{LUMO}\ (\text{eV}) \approx -1\text{e} \times [\ (E_{p,c}\ (\text{V vs Fc}^{+}|\text{Fc}) + 4.8\ (\text{V Fc}^{+}|\text{Fc vs zero})] \qquad (2)$$

while the distance between $E_{p,a}$ and $E_{p,c}$ affords calculation of the electrochemical HOMO–LUMO energy gap:

$$E_{g,\,EC}\ (\text{eV}) = -\ (E_{HOMO}\ (\text{eV}) - E_{LUMO}\ (\text{eV})) = 1\text{e} \times [E_{p,a}\ (\text{V vs Fc}^{+}|\text{Fc}) - E_{p,c}\ (\text{V vs Fc}^{+}|\text{Fc})] \qquad (3)$$

Such calculations can be made from both the peak maxima and the peak onsets, similarly to the spectroscopic case (a detailed discussion of the implications and meanings of such two approaches and of the third one based on formal potentials $E°$, not appliable to our specific case, is provided in Appendix C) . The results are reported in Table 3 together with the corresponding spectroscopic data. HOMO and LUMO energy levels are determined from, and account for, the combination of conjugation and inductive effects, and can be compared with those predicted by the theoretical computations (Table 2). This is conveniently achieved in Figure 5.

(Figure 5 here)

The most remarkable discrepancy in the two approaches concerns the HOMO levels, the electrochemical ones being much lower in energy than the theoretical ones. This difference should account for solvation effects, which appear significantly lower in the LUMO case. As a consequence, the theoretical HOMO-LUMO energy gaps are significantly narrower than the electrochemical ones. Moreover, a discrepancy is observed between the electrochemical energy gap sequence:

2,7 Th-Fluo-Th > 3,6 Th-Cbz-Th > 2,7 Th-Cbz-Th >>3,7 Th-Phen-Th

and the one predicted by computations:

3,6 Th-Cbz-Th > 2,7 Th-Cbz-Th > 2,7 Th-Fluo-Th > 3,7 Th-Phen-Th

This inversion arises from the HOMO of 2,7 Th-Fluo-Th being the one most stabilized upon solvation (compare Figure 5 (a) and (b)).

It is particularly interesting to remark that along both approaches, the theoretical and the experimental one, the kinking of the Cbz template results in both HOMO and LUMO energy levels rising (easier oxidation, more difficult reduction), albeit asymmetrically. In particular, the HOMO level rises less than the LUMO one, which may be a consequence of the decrease in conjugation on account of the structure bending (which should result in less stable radical cation and anion, and therefore in more extreme first oxidation and first reduction potentials, corresponding to lower

HOMO and higher LUMO) and the increase in localization of electron density on the central core (compare Figure 2), which should result in HOMO energy level rising, like in the limiting case of Phen. In this frame, the remarkable LUMO rising would be accounted for by the decrease in conjugation efficiency alone.

While theoretical HOMO and LUMO features display some differences with respect to the experimental electrochemical ones, the HOMO-LUMO energy gaps obtained by both experimental approaches (*i.e.* electrochemical and spectroscopic) are very similar and in a fairly linear relationship (Figure 6), albeit they do not coincide.

(Figure 6 here)

It is worthwhile to remark that some difference between optical and electrochemical data is often observed and quite reasonable, since optical data concern electron promotion between intramolecular levels, while the electrochemical information accounts for electron transfer between molecule and electrode, with concurrent formation of net positive or negative charges (Accordingly, also the solvent and supporting electrolyte effects can be significantly different in the two cases).

Unlike the LUMO and HOMO levels, the LUMO-HOMO energy gap is unaffected by substituent inductive effects (while regularly decreasing with increasing effective conjugation in the π system), excepting when the oxidation and reduction sites are significantly different. This can be surely assumed to be the case of 3,7 Th-Phen-Th, featuring peripheral LUMOs *vs* a HOMO centered on the phenothiazine core (as confirmed by theoretical computations and oxidative CV patterns), at a very high energy level as a consequence of the electron donating effect of the two heteroatoms. Accordingly the LUMO-HOMO gap undergoes an asymmetric shrinking, since the HOMO rises higher than the LUMO. This justifies the lowest position of 3,7 Th-Phen-Th in the LUMO-HOMO energy gap sequence:

2,7 Th-Fluo-Th > 3,6 Th-Cbz-Th > 2,7 Th-Cbz-Th >>3,7 Th-Phen-Th

notwithstanding its non-planar structure arising from the central core, which in itself should impair effective conjugation, with respect to the other templates.

Accordingly, it is worthwhile noticing that, in the same Figure 6, comparing the spectroscopic energy gaps of our monomers with those of the T_n linear oligothiophene series [75] taken as a reference and represented by vertical dash-and-dotted bars, all the points concerning cases in which both HOMO and LUMO are supposed to be delocalized on the whole molecule are clustered approximately midway between T_2 and T_3 (as if substitution of the core thiophene with a Fluo or Cbz unit slightly hampered the global effective conjugation) while the P_2 and P_3 gaps are significantly lower than the T_3 one, as a consequence of the above described asymmetric shrinking of the HOMO-LUMO gap.

3.3.2. Electropolymerization.

Changing the character of the fluorene core radically affects the polymerization ability of the monomers (Figure 7).

(Figure 7 here)

The parent term in the series, *i.e.* the one having a fluorene core, **F_1**, electropolymerizes, albeit slowly (confirming the radical cation to be at least partially localized in terminal α-thiophene positions, the only one available for polymerization in our monomer templates), with formation of a thin conducting layer, which however appears rather stable upon extraction from the monomer solution and subsequent stability tests in a monomer free one

Changing the all-C fluorene core with a phenothiazine one (**P_3** in Figure; **P_1** and **P_2** cases, not reported, have the same behaviour) the radical cation becomes completely localized in the heterocyclic core and highly stabilized by the electron-donating N and S heteroatoms. These two features, besides resulting in the above described shrinking of the LUMO-HOMO energy gap, completely hamper radical coupling, since no polymerization at all is observed even after many CV cycles (Figure 7) and at higher monomer concentrations (up to 0.001 M).

On the contrary, changing the all-C fluorene core with a carbazole core appears to powerfully promote polymerization, albeit with significant differences in the four cases considered:

a) both the 3,6 Th-Cbz-Th monomers that have an angular structure (**C'$_1$** and **C'$_2$**), polymerize faster than the linear 2,7 Th-Cbz-Th monomers (**C$_1$** and **C$_2$**) at constant cycle number, besides having a significantly lower first oxidation potential, as above accounted for; this feature appears consistent with a recent study of some of us on an intrinsically 3D multithiophene monomer, powerfully enhancing electropolymerization rates thanks to the central angle in the molecule [76]; moreover, the high dihedral angle hampering conjugation should result in more peripherally localized and therefore more reactive radical cations.

b) on the other side, the process involving the 2,7 Th-Cbz-Th monomers (**C$_1$** and **C$_2$**) appears more regioregular and selective, since the CV pattern looks narrower and sharper with respect to the broader **C'$_1$** and **C'$_2$** ones; this is consistent with the polymer growing in a single linear direction and therefore having less freedom degrees and 3D character with respect to the **C'$_1$** and **C'$_2$** cases;

c) An increasing bulkiness of the alkyl chain substituent(s) on the carbazole nitrogen atom appears to increasingly hamper polymerization, in terms of both smaller associated charge at constant cycle number, and above all higher oxidation potential (compare both **C'$_2$** with **C'$_1$,** and **C$_2$** with **C$_1$**). This effect, which only appears in the 3D process *i.e.* polymerization, while the CV features of the monomers in solution are nearly coincident, could be a consequence of the increasing length of the aliphatic chains resulting in (i) increasing solubility of the oligomers, and/or (ii) increasing difficulty in 3D ordering during film formation (also resulting in weaker π stacking effects), and/or (iii) decreasing probability of effective encounters between radical cations to give coupling and therefore polymerization. This is fully consistent with former observations by some of us in a comparative study on substituted thiahelicenes [70].

A remarkable behaviour has been observed in the case of polymer C_2, growing at more positive potentials than C_1, but progressively attaining the same less positive onset oxidation potential upon transfer in a monomer-free solution and subsequent repeated cycling in a potential range

including charge trapping (Figure 8). This could point to progressively better packing of the polymer chains fostered by the cyclic "pulsation" of the solid state film implied by the charge trapping phenomenon; this would result in progressively more efficient π-stacking interactions and therefore more effective overall conjugation. In this light, the hampering effect of the alkyl substituent on the conjugation improvement achievable upon polymerization should be considered of a kinetic rather than a thermodynamic character.

(Figure 8 here)

3.3.3. Electrochemistry of the polymers.

Figure 8 provides a synopsis of CV characteristics for the polymers obtained from the four monomer templates along three different pathways:

a) Electropolymerization on GC electrodes from a 0.0002 M-0.00025 M solution, by repeated cycling (48 cycles) around the first oxidation peak in ACN + 0.1 M TBATFB;

b) $FeCl_3$-oxidative polymerization, followed by polymer dissolution in $CHCl_3$, deposition of a drop of the resulting solution on the GC surface, and finally characterization of the film-coated electrode in the same above medium;

c) Pd-catalyzed chemical polymerization *via* Suzuki coupling, followed by polymer dissolution in $CHCl_3$ at constant concentration (1 mg cm^{-3}), deposition of 0.2 cm^3 of the resulting solution on the GC surface, and finally characterization of the film-coated electrode in the same above medium.

The CV patterns provided are stationary ones, obtained after 5-10 potential cycles. Actually not only the polymer films are stable upon cycling, but they appear to attain full redox activity (maximum current, lowest oxidation/reduction potentials, peak features pointing to facile electron transfer) only after some conditioning by repeated potential cycling. This is consistent with the chemically synthesized polymers needing to give off residuals of chemicals from the synthetic step and to condition their networks in the new medium, which can be different from the one employed

in the synthetic step. Actually the film structure and performance should be significantly affected by both solvent and supporting electrolyte, the ions from the latter having to cyclically enter/exit the solid phase.

For sake of comparison, HOMO and LUMO energy levels and gaps for the polymers obtained by Suzuki coupling are contrasted with the monomer ones in Figure 5c. It appears that, consistently with the polymer data collected in Table 5, polymerization results in narrower HOMO-LUMO energy gaps, which is a usual feature originating from increased effective conjugation both as a consequence of the increased number of conjugated aromatic rings and/or of solid-state π-stacking 3D interactions.

(Table 5 here)

However, it is interesting to notice that, as it is evident in Figure 5c, in all the present cases the narrower gaps are much more the consequence of the (remarkable) positive shift of the reduction potentials than of the (very little) negative shift of the oxidation potentials. Actually in the phenothiazine case the oxidation potential of the monomer is even less positive than the corresponding polymer one. Therefore changing thiophene units with bithiophene ones appears to contribute much more to radical anion stabilization than to radical cation one. This is indeed expected in the Phen case, considering the assumed localization of the radical cation in the phenothiazine core and delocalization of the radical anion; but it looks to hold for the other templates, too, including the Fluo one, which has no donating heteroatom on the core. Actually the polymer obtained by Suzuki coupling of a [Th-Fluo] unit, resulting in thiophene spacers instead of bithiophene ones, shows a remarkable decrease in the radical anion stabilization ability, while the oxidation pattern is perfectly superimposable to the Th-Fluo-Th case with bithienyl units (Figure 9).

(Figure 9 here)

The highest improvement in charge stabilization ability upon polymerization (most significant shrinking of the energy gap) is obtained for the linear carbazole template.

It is worthwhile noticing that while electrochemical and spectroscopical gaps nearly coincide in the monomer case (empty symbols in Figure 6, lying on the bisector), the corresponding polymer ones are remarkably higher when calculated from CV data with respect to the UV-Vis ones (full symbols in the same Figure 6, far away from the bisector). This feature should account for some solid-state effect differently affecting the electrochemical process with respect to the spectroscopic one, in particular the additional energy possibly required for the counterion entering and exiting the polymer network, in order to balance the net charge creation.

Figure 6 also evidences that the polymers obtained from the angular C'1 and C'2 monomers have lower effective conjugation than the polymers obtained from all the linear monomers, albeit they grow much more rapidly. This could be a consequence of lower planarity and lower π-stacking effects (implied by the angular structure), both hampering effective conjugation, and lower regioregularity (as a consequence of the high polymerization rate).

Comparison between the electrochemical polymers, which have been obtained in constant conditions, shows that (Figure 8):

- in the phenothiazine case, a polymer could be obtained only by the Suzuki coupling, while both electro- and oxidative ($FeCl_3$) polymerizations were not observed in our operating conditions; this is reasonable, since both routes hinge on a reactive radical cation intermediate.
- the angular carbazole monomer is by far the aptest to polymerization, the corresponding polymer having the highest peak current and charge;
- The carbazole cases afford evaluation of the effect on the polymer film properties of both branching (C'_2 *vs* C'_1) and increasing bulkiness (C_2 *vs* C_1) of the alkyl chain substituent on the nitrogen atom. Consistently with a recent study [77], both features, popular tools to improve solubility of the starting monomer, also appear to significantly affect the electronic properties of the film in the solid state, resulting in a slight but perceivable hampering effect on the electron transfer processes, both oxidative and

reductive; this effect could be associated with a less tightly packed 3D structure (resulting in smaller π-stacking effects) and/or with increasingly hampered electron tunnelling between the redox sites in the polymer network and the electrode surface.

- All the polymers have charge trapping ability, implying cyclic structural modifications of the solid state films; in the case of C_2 such phenomenon apparently fostered optimization of 3D packing and therefore enhancement of π-stacking effects.

3.4. AFM imaging

The morphology of the electrosynthesized polymers $[C_1]_n$, $[C'_1]_n$, and $[F_1]_n$ was investigated by Atomic Force Microscopy (AFM); phase images and sections are reported in Figure 10.

The three samples were obtained in the same conditions, by electropolymerization on ITO glass from a 0.0002 M-0.0004 M solution of the monomer in ACN + 0.1 M TBATFB, by repeated cycling (48 cycles) around the first oxidation peak (see paragraph 2.4).

The polymerization ability of the precursor monomers reflects on the morphology of the resulting polymers: the three samples differ in both particle dimension and surface roughness. The C'_1 high polymerization rate ensues big particles, with a diameter of 150-200 nm and 100 nm height, while the opposite behaviour of F_1 leads to formation of the smallest particles in the series (30-40 nm diameter, 10-15 nm height). As expected from CV evidence, the morphology of $[C_1]_n$ is regular and the polymer grows in a single direction: particles have a diameter of 90-100 nm, but the height is between 15-20 nm.

(Figure 10 here)

4. Conclusions

Our exhaustive comparative investigation affords a series of reliable guidelines concerning the relationships between molecular structure, electronic properties and polymerization ability.

Heteroatoms in the core ring. Gradually increasing the electron richness of the X core by adding N and/or S heteroatoms (Fluo<Cbz<Phen) chiefly affects the HOMO energy, which regularly rises; this implies a less positive potential for radical cation formation, a desirable feature for electropolymerization, and also a smaller energy gap, provided that the LUMO is considerably less affected by the X core than the HOMO. While rising in energy, however, the HOMO increasingly concentrates on the X core as a consequence of the electron donating effect of the heteroatom(s), and for the same reason the forming radical cation is increasingly localized and stabilized on the X core.

Kinked vs linear structure. Changing the positions of the side thiophene units to obtain a kinked structure instead of a linear one results in loss of conjugation efficiency for both monomer and polymer; the central angle however affords a less negative oxidation potential and a remarkable increase in the polymerization rate possibly linked to more peripherally localized and therefore more reactive radical cation intermediates. On the contrary, a linear structure with less 3D attitude, polymerizes at a more positive potential and more slowly, but with a considerable increase in regularity and effective conjugation of the conducting film.

Alkyl substituents. The bulkiness and branching of alkyl substituents possibly added on the core *e.g.* to improve solubility for industrial processing increasingly hampers radical cation formation on the polymer, while resulting nearly uninfluential on the monomer; this could be due to increasing difficulty in 3D ordering during film formation, weaker π-stacking effects and/or decreasing probability of effective encounters between radical cations.

Scaffold rigidity. The most rigid Fluo structure has the by far lowest Stokes shift together with a nearly quantitative quantum yield; increasingly adding heteroatoms on the core and/or introducing structure bending, like in the Phen and kinked Cbz cases, tends to favour non-radiative decay

pathways with a consequent decrease in quantum yields and results in increasing Stokes shifts, due to a more pronounced difference between the ground and excited state energy curves as a function of the nuclear coordinates.

Polymerization routes. Alternative polymerization pathways proved nearly equivalent. The electrochemical approach is somehow more selective, proving uneffective in the above peculiar Phen case at least at our moderate operating monomer concentrations. The same holds for the oxidative $FeCl_3$ route. The Suzuki coupling approach proved the most generally applicable one.

The systematic template sequence combined with the rigorous, multitechnique protocol make the above rationalization criteria reliable and of general application in the Th-X-Th semiconductor class; in the same time a unique systematic data library has been made available for these molecules. Both features could provide useful support for their target-oriented design and use, both as such and as building blocks for multicomponent electroactive functional materials.

References

[1] R. Po, M. Maggini, N. Camaioni, J. Phys. Chem. C 114 (2010) 695.

[2] K. S. Liao, S. D. Yambem, A. Haldar, N. J. Alley, S. A. Curran, Energies 3 (2010) 1212.

[3] M. A. Uddin, H.P. Chan, B.M.A. Rahman, Rev.Adv.Mater.Sci. 26 (2010) 58.

[4] R. Kroon, M. Lenes, J. C. Hummelen, P. W. M. Blom, B. De Boer, Polym. Rev., 48 (2008) 531.

[5] J. Chen, Y. Cao, Acc. Chem. Res., 42 (2009) 1709.

[6] P. T. Boudreault, A. Najari, M. Leclerc, Chem. Mater. 23 (2011) 456.

[7] J. M. Szarko, J. Guo, B. S. Rolczynski, L. X. Chen, J. Mater. Chem. DOI: 10.1039/c0jm04433d

[8] D. Gendron, M. Leclerc, Energy Environ. Sci. 4 (2011) 1225.

[9] C.J. Brabec, A. Cravino, D. Meissner, N.S. Sariciftci, T. Fromherz, M.T. Rispens, L. Sanchez, J.C. Hummelen, Adv. Funct. Mater.11 (2001) 374.

[10] S.A., Choulis, Y. Kim, J. Nelson, D.D.C. Bradley, M., Giles, M. Shkunov, I. McCulloch, Appl. Phys. Lett. 85 (2004) 3890.

[11] F.C. Krebs, Sol. Energy Mat. Sol. Cells 93 (2009) 394.

[12] M. Svensson, F. Zhang, O. Inganäs, M.R. Andersson, Synth. Met. 135-136 (2003) 137.

[13] M. Svensson, F. Zhang, S.C.Veenstra, W. J. H. Verhees, J. C. Hummelen, J. M. Kroon, O. Inganäs, M. R. Andersson, Adv. Mater. 15 (2003) 988.

[14] O. Inganäs, M. Svensson, F. Zhang, A. Gadisa, N. K. Persson, X. Wang, M. R. Andersson, Appl. Phys. A: Mat. Sci. Proc. 79 (2004) 31.

[15] L. Bonoldi, A. Calabrese, A. Pellegrino, N. Perin, R. Po, S. Spera, A. Tacca, J. Mater. Sci. 46 (2011) 3960.

[16] L. M. Andersson, O. Inganäs, Appl. Phys. Lett. 88 (2006) 082103.

[17] S. Admassie, O. Inganäs, W. Mammo, E. Perzon, M.R. Andersson, Synth. Met. 156 (2006) 614.

[18] A. Gadisa, W. Mammo, M. Andersson, S. Admassie, F. Zhang, M.R. Andersson, O. Inganäs, Adv. Funct. Mater. 17 (2007) 3836.

[19] M. Karikomi, C. Kitamura, S. Tanaka, Y. Yamashita, J. Am. Chem. Soc. 117 (1995) 6791.

[20] H.A.M. van Mullekom, J.A.J.M. Vekemans, E.W. Meijer, Chem. Eur. J. 4 (1998) 1235.

[21] Q. Hou, Y. Xu, W. Yang, M. Yuan, J. Peng, Y. Cao, J. Mater. Chem. 12 (2002) 2887.

[22] C. J. Brabec, C. Winder, N.S. Sariciftci, J.C. Hummelen, A. Dhanabaln, P. Van Hal, R.A.J. Janssen, Adv. Funct. Mater. 12 (2002) 709.

[23] M. Chen, E.Perzon, M.R. Anderson, S. Marcinkevicius, S.K.M. Jönsson, M. Fahlman, M. Berggren, Appl. Phys. Lett. 84 (2004) 3570.

[24] R. Yang, R. Tian, J. Yan, Y. Zhang, J. Yang, Q. Hou, W. Yang, C. Zhang, Y. Cao, Macromolecules 38 (2005) 244.

[25] M Velusamy, K.R.J. Thomas, J.T. Lin, Y.C. Hsu, K.C. Ho, Org. Lett. 7 (2005) 1899.

[26] E. Bundgaard, F.C. Krebs, Macromolecules 39 (2006) 2823.

[27] M Shahid, RS Ashraf, E Klemm, S. Sensfuss, Macromolecules 39 (2006) 7844.

[28] Z. Zhu, D. Waller, R. Gaudiana, M. Morana, D. Mühlbacher, M. Scharber, C.J. Brabec, Macromolecules 40 (2007) 1981.

[29] N. Blouin, A.Michaud, D.Gendron, S.Wakim, E.Blair, R.Neagu-Plesu, M.Belletete, G. Durocher, Y.Tao, M. Leclerc, J. Am. Chem. Soc. 130 (2008) 732.

[30] N. Blouin, A. Michaud, M. Leclerc, Adv. Mater. 19 (2007) 2295.

[31] N. Blouin, M. Leclerc, Acc. Chem. Res. 41 (2008) 1110.

[32] S.H. Park, A. Roy, S. Beaupré, S. Cho, N. Coates, J. S. Moon, D. Moses, M. Leclerc, K. Lee, A.J. Heeger, Nature Photonics 3 (2009) 297.

[33] W. Pisula, A.K. Mishra, J. Li, M. Baumgartner, K. Mullen in: C.J. Brabec, V. Dyakonov, U. Scherf (eds.), Organic photovoltaics. Materials, device physics and manufacturing technologies; Wiley-VCH: Weinheim, 2008, 93-128.

[34] W. Tang, T. Kietzke, P. Vemulamada, Z.-K. Chen, J. Polym. Sci., Polym Chem Ed. 45 (2007) 5266.

[35] J. Sakamoto, M. Rehahn, G. Wegner, A.D. Schlüter, Macromol. Rapid Commun. 30 (2009) 653.

[36] R. Sugimoto, S. Takeda, H. B. Gu, K. Yoshino, Chem. Express, 1 (1986) 635.

[37] R.G. Parr, W. Yang (eds.), Density-Functional Theory of Atoms and Molecules, Oxford University Press, Oxford, 1994.

[38] C. Fonseca Guerra, O. Visser, J.G. Snijders, G. te Velde, E.J. Baerends, in: E. Clementi, G. Corongiu (eds.), Methods and Techniques for Computational; STEF, Cagliari, 1995.

[39] G. te Velde, F.M. Bickelhaupt, E. J. Baerends, S. J. A. van Gisbergen, C. Fonseca Guerra, J.G. Snijders, T. Ziegler, J. Comput. Chem. 22 (2001) 931.

[40] E.J. Baerends, D.E. Ellis, P. Ros, Chem. Phys. 2 (1973) 41.

[41] E.J Baerends, P. Pos, Chem. Phys. 2 (1973) 52.

[42] C. Fonseca Guerra, J.G. Snijders, G. te Velde, E.J. Baerends, Theoretical Chemistry Accounts 99 (1998) 391.

[43] ADF2009.01, SCM, E.J. Baerends et al., Amsterdam Density Functional, Theoretical Chemistry, Vrije Universiteit, Amsterdam, URL http://www.scm.com.

[44] J.C. Slater, Phys. Rev. 36 (1930) 57.

[45] T. Ziegler, A. Rauk, Theor. Chim. Acta 46 (1977) 1.

[46] F. E. Harris, H.H. J. Michels, Chem. Phys. 45 (1966) 116.

[47] E. Filter, E.O. Steinborn, Phys. Rev. A 18 (1978) 1.

[48] S. H. Vosko, L. Wilk, M. Nusair, Can. J. Phys. 58 (1980) 1200.

[49] J.P. Perdew, Phys. Rev. B 33 (1986) 8822.

[50] A.D. Becke, Phys. Rev. A 38 (1988) 3098.

[51] A.D. Becke, J. Chem. Phys. 98 (1993) 5648.

[52] C. Lee, W. Yang, R.G. Parr, Phys. Rev. B 37 (1988) 785.

[53] S.J.A. van Gisbergen, J. G. Snijders, E. J. Baerends, J. Chem. Phys. 103 (1995) 9347.

[54] S.J.A. van Gisbergen, J. G. Snijders, E. J. Baerends, Comput. Phys. Commun. 118 (1999) 119.

[55] S.J.A. van Gisbergen, C. Fonseca-Guerra, E. J. Baerends, J. Comput. Chem. 21 (2000) 1511.

[56] F. Furche, R. Ahlrichs, C. Wachsmann, E. Weber, A. Sobanski, F. Vögtle, S. Grimme, J. Am. Chem. Soc. 122 (2000) 1717.

[57] J. Autschbach, T. Ziegler, S.J.A. van Gisbergen, E.J. Baerends, J. Chem. Phys. 116 (2002) 6930.

[58] J. Autschbach, T. Ziegler, J. Chem. Phys. 116 (2002) 891.

[59] W. Kohn, L.J. Sham, J. Phys. Rev. 140 (1965) A1133.

[60] Izmaylov A. F. Izmaylov, V. N. Staroverov, G. E. Scuseria, E. R. Davidson, G. Stoltz, E. Cancès, J. Chem. Phys. 126 (2007) 084107.

[61] G. Gritzner, J. Kuta, Pure Appl. Chem. 56 (1984) 461.

[62] A. J. Bard, L. R. Faulkner, Electrochemical Methods. Fundamentals and Applications (2nd edition); Wiley: New York, 2001, 648-650.

[63] J. Bouchard, M. Belletête, G. Durocher, M Leclerc, Macromolecules 36 (2003) 4624.

[64] L.Yang, J. Kang Feng, A.-M. Ren, J. Org. Chem. 70 (2005) 5987.

[65] M. Belletête, J. Bouchard, M. Leclerc, G. Durocher, Macromolecules 38 (2005) 880.

[66] M. Bernius, M. Inbasekaran, E. Woo, W. Wu, L. Wujkowski, J. Mater. Sci.-Mater. Electron. 11 (2000) 111.

[67] H. Shao, X. Chen, Z. Wang, P. Lu, J. Lumin. 127 (2007) 349.

[68] J.-M. Savéant, Elements of Molecular and Biomolecular Electrochemistry Wiley: New Jersey, 2006,80-92.

[69] = Ref. [68], 102-106.

[70] A. Bossi, L. Falciola, C. Graiff, S. Maiorana, C. Rigamonti, A. Tiripicchio, E. Licandro, P.R. Mussini, Electrochim. Acta 54 (2009) 5083.

[71] T. Benincori, V. Bonometti, F. De Angelis, L. Falciola, M. Muccini, P.R. Mussini, T. Pilati, G. Rampinini, S. Rizzo, S.Toffanin, F. Sannicolò, Chemistry, a European Journal 16 (2010) 9086.

[72] W.-Y.Wong, X.-Z. Wang, Z. He, A. B. Djurisic, C.-T.Yip, K.-Y.Cheung, H. Wang, C. S. K. Mak, W.-K. Chan, Nature Materials, 6 (2007) 521.

[73] R. S. Ashraf, M. Shahid, E. Klemm, M. Al-Ibrahim, S. Sensfuss, Macromol. Rapid Commun. 27 (2006) 1454.

[74] S. Trasatti, Pure Appl. Chem. 58 (1986) 955.

[75] C. Ma, E. Mena-Osteriz, T. Debaerdemaeker, M.M. Wienk, R.A.J. Janssen, P. Bauerle, Angew.Chem. Int. Ed. 46 (2007) 1679.

[76] F. Sannicolò, S. Rizzo, T. Benincori, W. Kutner, K. Noworyta, J. W. Sobczak, V. Bonometti, L. Falciola, P. R. Mussini, M. Pierini, Electrochim. Acta 55 (2010) 8352.

[77] L. Yang, H. Zhou; W. You, J. Phys. Chem C 114 (2010) 16793

Table 1. Theoretical data of HOMO, LUMO, and HOMO-LUMO energy gaps, for different Th-X-Th templates. The shadowed lines indicate the templates corresponding to experimentally investigated monomers.

structure	charge	spin	E_{HOMO} /eV	E_{LUMO} /eV	E_{gap} /eV
3,6 Th–Fluo–Th	**0**	**0**	**-5.18**	**-2.10**	**3.07**
	0	2	-2.62	-4.71	-2.10
	1	1	-8.39	-8.24	0.16
	-1	1	0.80	0.97	0.18
2,7 Th–Fluo–T h	**0**	**0**	**-4.93**	**-2.47**	**2.46**
	0	2	-2.96	-4.47	-1.51
	1	1	-8.15	-7.92	0.23
	-1	1	0.44	0.66	0.22
3,6 Th–Cbz–Th	**0**	**0**	**-4.78**	**-2.02**	**2.76**
	0	2	-2.53	-4.24	-1.72
	1	1	-8.12	-7.87	0.25
	-1	1	0.96	1.16	0.20
2,7 Th–Cbz–Th	**0**	**0**	**-4.92**	**-2.38**	**2.54**
	0	2	-2.86	-4.47	-1.61
	1	1	-8.15	-7.91	0.23
	-1	1	0.53	0.75	0.22
2,8 Th–Phen– Th	**0**	**0**	**-4.60**	**-2.22**	**2.37**
	0	2	-2.69	-4.22	-1.52
	1	1	-8.00	-7.71	0.28
	-1	1	0.61	0.78	0.17
3,7 Th–Phen– Th	**0**	**0**	**-4.57**	**-2.19**	**2.38**
	0	2	-2.64	-4.20	-1.56
	1	1	-7.85	-7.59	0.26
	-1	1	0.64	0.86	0.22

Table 2. Calculated molecular dipole moments and their Cartesian components (Debye) for the four investigated monomer templates.

molecule	μ_{tot} / D	μ_X / D	μ_Y /D	μ_Z /D
2,7 Th–Fluo–T h	1.01	-0.80	-0.33	0.51
3,6 Th–Cbz–Th	2.47	0.64	-2.38	0.21
2,7 Th–Cbz–Th	2.34	0.58	-2.10	-0.84
3,7 Th–Phen– Th	2.554	0.59	0.92	2.30

Table 3. Experimental data of HOMO, LUMO, and HOMO-LUMO energy gaps, obtained from UV-Vis absorption peaks or electrochemical first oxidation and reduction peaks using either the onset or the maxima criterion. The working solvent (ACN = acetonitrile or DCM = dichloromethane) is reported as a superscript, the supporting electrolyte being 0.1 M TBATFB for all electrochemical experiments.

Template	2,7 Th–Fluo–Th	3,6 Th–Cbz–Th	2,7 Th–Cbz–Th	3,7 Th–Phen– Th
		Onset criterion		
$E_{HOMO\ EC}$ /eV	F_1 −5.56^{ACN}	C'_1 −5.20^{ACN} C'_2 −5.22^{ACN}	C_1 −5.41^{ACN} C_2 −5.32^{ACN}	P_1 −4.97^{ACN} P_2−5. 02^{ACN} P_3 −5.04^{ACN}
	F_1 −5.50 ^{DCM}	C'_1 −5.23^{DCM}	C_1 −5.29^{DCM}	
$E_{LUMO\ EC}$ /eV	F_1 −2.22 ^{ACN}	C'_1 −1.97 ^{ACN} C'_2 −1.98^{ACN}	C_1 −2.24^{ACN} C_2 −2.23^{ACN}	P_1 −2.03^{ACN} P_2 −2.04^{ACN} P_3 −2.04^{ACN}
$E_{gap\ EC}$/eV	F_1 3.34 ^{ACN}	C'_1 3.23 ^{ACN} C'_2 3.24^{ACN}	C_1 3.17^{ACN} C_2 3.09^{ACN}	P_1 2.94 ^{ACN} P_2 2.98^{ACN} P_3 3.00 ^{ACN}
$E_{gap\ UV}$ /eV	F_1 3.25^{ACN}	C'_1 3.24^{ACN} C'_2 3.19^{ACN}	C_1 3.19^{ACN} C_2 3.19^{ACN}	P_2 2.94^{ACN} P_3 2.92^{ACN}
	F_1 3.22 ^{DCM}	C'_1 3.20 ^{DCM} C'_2 3.20^{DCM}	C_1 3.16^{DCM} $C_2$3.17^{DCM}	P_1 2.84^{DCM} P_2 2.93^{DCM} P_3 2.93^{DCM}
		Maxima criterion		
$E_{HOMO\ EC}$ /eV	F_1 −5.66^{ACN}	C'_1 −5.37^{ACN} C'_2 −5.39^{ACN}	C_1 −5.51^{ACN} C_2 −5.42^{ACN}	P_1 −5.10^{ACN} P_2 −5.14^{ACN} P_3 −5.16^{ACN}
	F_1 −5.63 ^{DCM}	C'_1 −5.37^{DCM}	C_1 −5.59^{DCM}	
$E_{LUMO\ EC}$ /eV	F_1 −2.12 ^{ACN}	C'_1 −1.79 ^{ACN} C'_2 −1.81^{ACN}	C_1 −2.02^{ACN} C_2 −2.02^{ACN}	P_1 −1.94^{ACN} P_2 −1.91^{ACN} P_3 −1.92^{ACN}
$E_{gap\ EC}$/eV	F_1 3.54^{ACN}	C'_1 3.58 ^{ACN} C'_2 3.58^{ACN}	C_1 3.49^{ACN} C_2 3.40^{ACN}	P_1 3.16^{ACN} P_2 3.23^{ACN} P_3 3.24^{ACN}
$E_{gap\ UV}$ /eV	F_1 3.54^{ACN}	C'_1 3.97^{ACN} C'_2 3.96^{ACN}	C_1 3.53^{ACN} C_2 3.53^{ACN}	P_2 3.46^{ACN} P_3 3.43^{ACN}
	F_1 3.52 ^{DCM}	C'_1 3.95 ^{DCM} C'_2 3.95^{DCM}	C_1 3.50^{DCM} C_2 3.51^{DCM}	P_1 3.48^{DCM} P_2 3.43^{DCM} P_3 3.44^{DCM}

Table 4. Quantum yields QY and lifetimes τ for the emission peaks in ACN. The wavelengths of excitation (λ_{exc}) are also reported.

structure	QY (λ_{exc} / nm)	τ / ns
2,7 Th–Fluo–Th	78.6 (350)	1.06
3,6 Th–Cbz–Th	3.3 (340)	1.61
2,7 Th–Cbz–Th	37.2 (350)	2.80
3,7 Th–Phen– Th	13.7 (352)	1.67

Table 5. Experimental data of HOMO, LUMO, and HOMO-LUMO energy gaps of the polymer films obtained from UV-Vis absorption peaks or electrochemical first oxidation and reduction peaks using the onset criterion.

structure	synthetic route	$E_{HOMO\ EC}$ /eV	$E_{LUMO\ EC}$ /eV	$E_{gap\ EC}$ /eV	$E_{gap\ UV}$ /eV
$[F_1]_n$ – [Th–Fluo–Th]$_n$– (2,7)	Electrochemical polymerization	-5.31	-2.64	2.67	-
	Suzuki polymerization	-5.49	-2.60	2.89	2.34
	Oxidative polymerization	-5.44	-2.57	2.87	2.41
$[f_1]_n$ – [Th–Fluo]$_n$– (2,7)	Suzuki polymerization	-5.52	-2.31	3.21	2.55
$[C'_1]_n$ –[Th–Cbz–Th]$_n$– (3,6)	Electrochemical polymerization	-5.16	-2.25	2.91	2.51
	Oxidative polymerization	-5.20	-2.40	2.80	2.52
$[C'_2]_n$ –[Th–Cbz–Th]$_n$– (3,6)	Electrochemical polymerization	-5.39	-2.07	3.32	-
	Suzuki polymerization	-5.20	-2.17	3.03	2.51
$[C_1]_n$ –[Th–Cbz–Th]$_n$– (2,7)	Electrochemical polymerization	-5.09	-2.47	2.62	2.27
$[C_2]_n$ –[Th–Cbz–Th]$_n$– (2,7)	Electrochemical polymerization	-5.22	-2.50	2.72	-
	Suzuki polymerization	-5.20	-2.49	2.71	2.32
$[P_3]_n$ –[T–PhT– T]$_n$– (3,7)	Suzuki polymerization	-5.17	-2.41	2.76	2.42

FIGURE LEGENDS

Figure 1. A synopsis of the investigated Th-X-Th monomers.

Figure 2. Calculated HOMO and LUMO orbitals for six template structures (fundamental state).

Figure 3. Typical absorption and emission spectra in ACN solvent of the four experimentally investigated monomer templates. (a) 2,7 Th-Fluo-Th (monomer $\mathbf{F_1}$); (b) 2,7 Th-Cbz-Th (monomer $\mathbf{C_1}$); (c) 3,7 Th-Phen-Th (monomer $\mathbf{P_3}$); (d) 3,6 Th-Cbz-Th (monomer $\mathbf{C'_1}$). Vertical bars represent the relative oscillator strengths for the most relevant theoretical transitions predicted by excitation analysis.

Figure 4. A synopsis of CV features recorded for the eight investigated monomers in ACN + 0.1 M TBATFB medium, on GC electrode, at 0.2 V s^{-1}. Potentials are referred to the $Fc^+|Fc$ intersolvental reference redox couple.

Figure 5. HOMO and LUMO energy levels and LUMO-HOMO energy gaps for the four templates. (a): from theoretical computations on the methylated monomer templates in vacuum; (b): from the electrochemical experiments in ACN medium, calculated along the onset criterion, with the four templates being represented by monomers F_1, C_1, C'_1 (dot lines), P_3; (c): from the corresponding polymers synthesized by Suzuki coupling and deposited on GC electrode.

Figure 6. Relationship between electrochemical and spectroscopic LUMO-HOMO energy gaps, calculated along the onset criterion, for the six monomers F_1 (empty circle), C'_1 and C'_2 (empty diamonds), C_1 and C_2 (empty squares), P_2 and P_3 (empty triangles) and the corresponding polymers $[F_1]_n$ (full circle), $[C'_1]_n$ and $[C'_2]_n$ (full diamonds), $[C_1]_n$ and $[C_2]_n$ (full squares), and $[P_3]_n$ (full

triangle). Spectroscopic energy gaps for selected α-linear oligothiophenes $\mathbf{T_n}$ (with n thiophene units) are also reported as vertical bars, for sake of comparison.

Figure 7. Electropolymerization cycles for different Th-X-Th monomers (0.0002–0.0004 M in ACN + 0.1 M TBATFB), and subsequent stability test in monomer-free solutions, on GC electrode, at 0.2 V s^{-1} potential scan rate.

Figure 8. Synopsis of redox properties (in ACN + 0.1 M TBATFB monomer-free solutions, on GC electrode, at 0.2 V s^{-1}) of conducting polymers representing our four Th-X-Th templates, synthesized along three different routes: Suzuki coupling, $FeCl_3$ oxidative polymerization and/or electropolymerization. To account for the effect of different alkyl substituents on the nitrogen atom, two cases are reported for both the 3,6 Th-Cbz-Th and the 2,7 Th-Cbz-Th templates, contrasting $[C'_1]_n$ vs $[C'_2]_n$ (in separate rows) and $[C_1]_n$ vs $[C_2]_n$ (as superimposed dotted and solid lines, respectively).

Figure 9. Contrasting the redox behaviour of $[2.7\ Th–Fluo–Th]_n$ and $[2\ Th–Fluo]_n$ polymers, both synthesized by the Suzuki coupling route and deposited on GC electrodes. CV patterns are recorded in ACN + 0.1 M TBATFB monomer-free solutions, at 0.2 V s^{-1}.

Figure 10. AFM imaging and profiling of polymer film surfaces, obtained by electropolymerization of monomer:

(a) $\mathbf{C'_1}$ (48 cycles) from a 0.00034 M solution in ACN + 0.1 M TBATFB, on ITO electrode;

(b) $\mathbf{C_1}$ (48 cycles) from a 0.00022 M solution in ACN + 0.1 M TBATFB, on ITO electrode;

(c) $\mathbf{F_1}$ (48 cycles) from a 0.00030 M solution in ACN + 0.1 M TBATFB, on ITO electrode.

Figure 1.

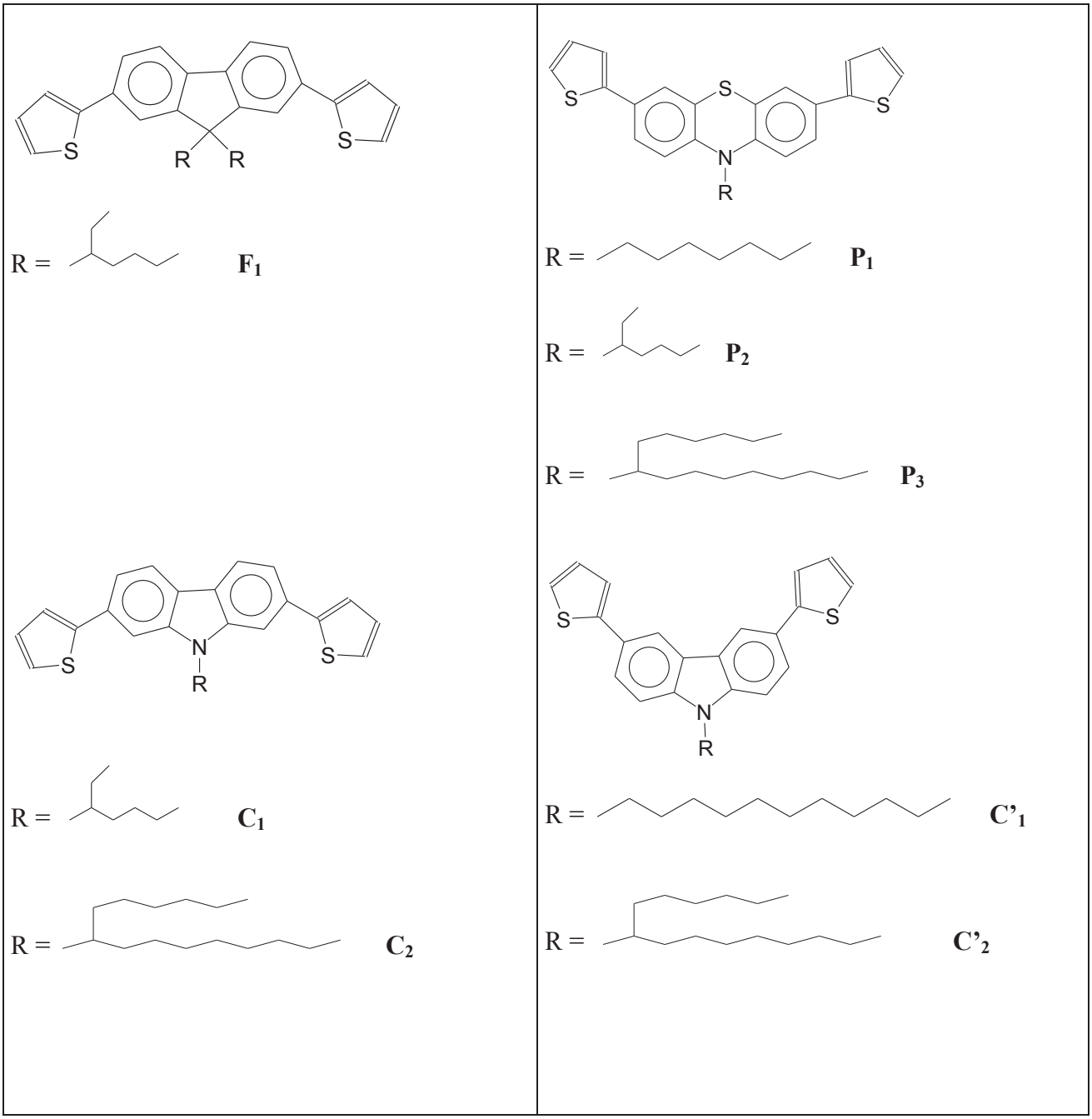

Figure 2. Web version

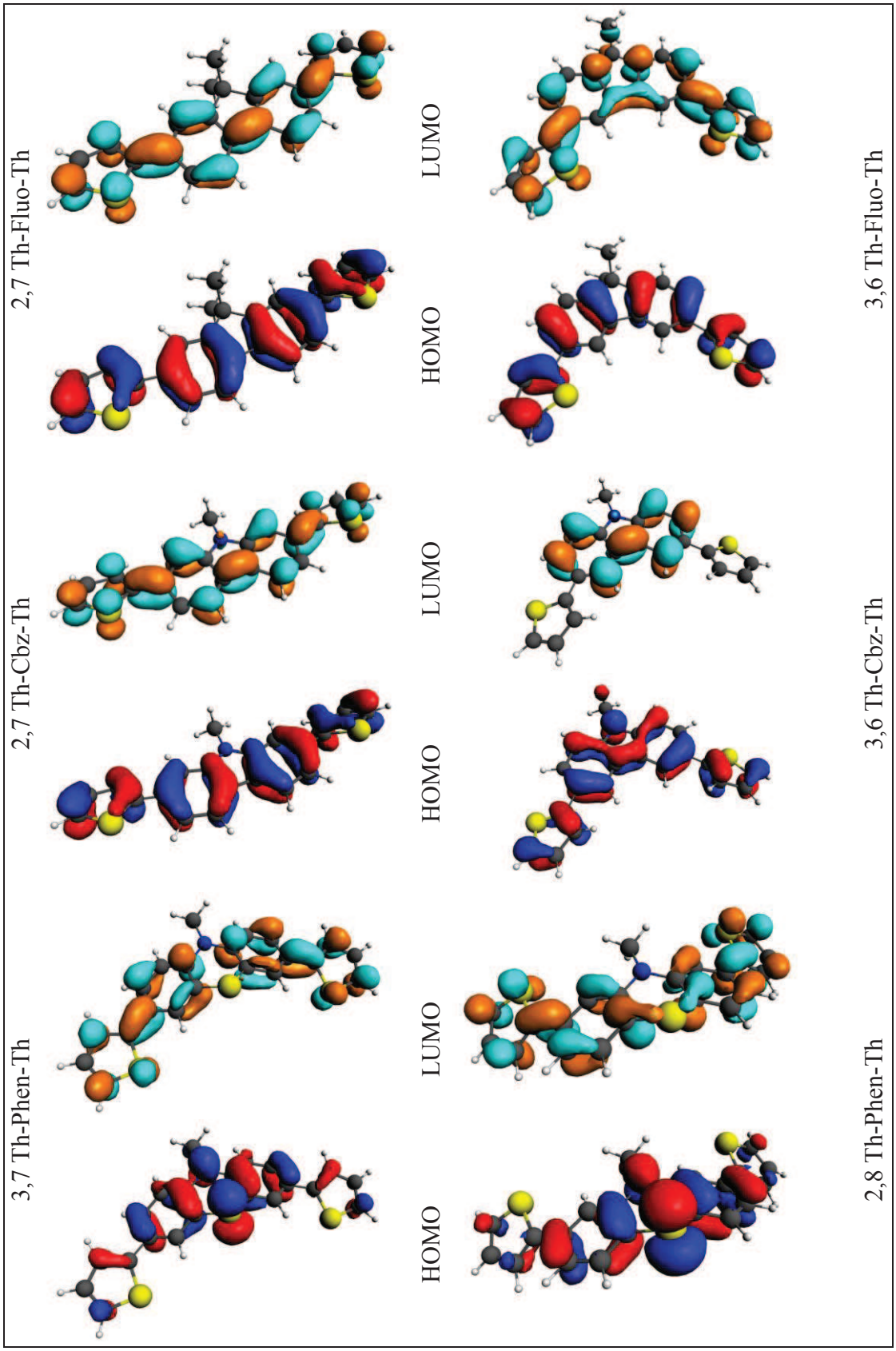

Figure 2. Print version

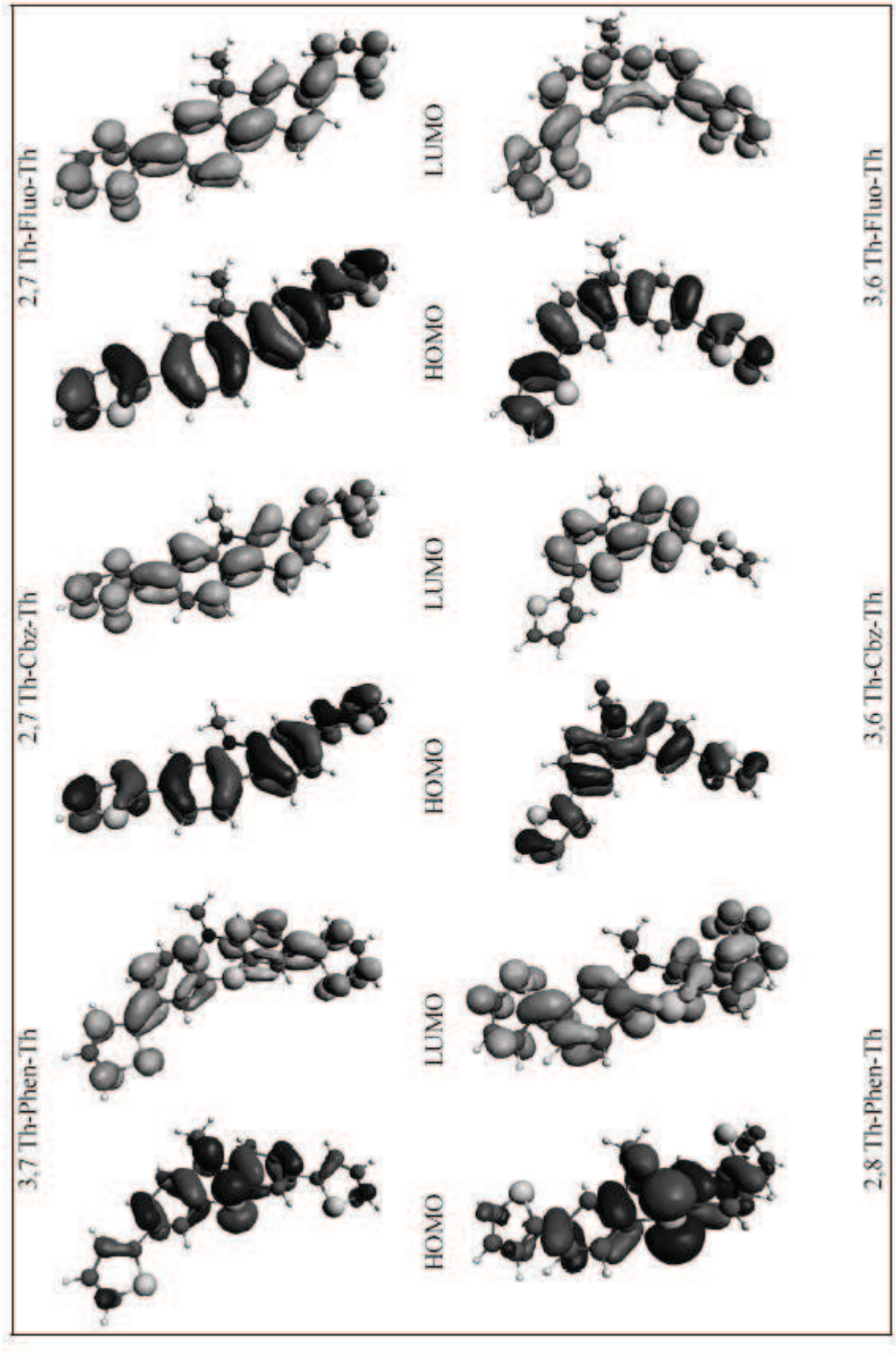

Figure 3.

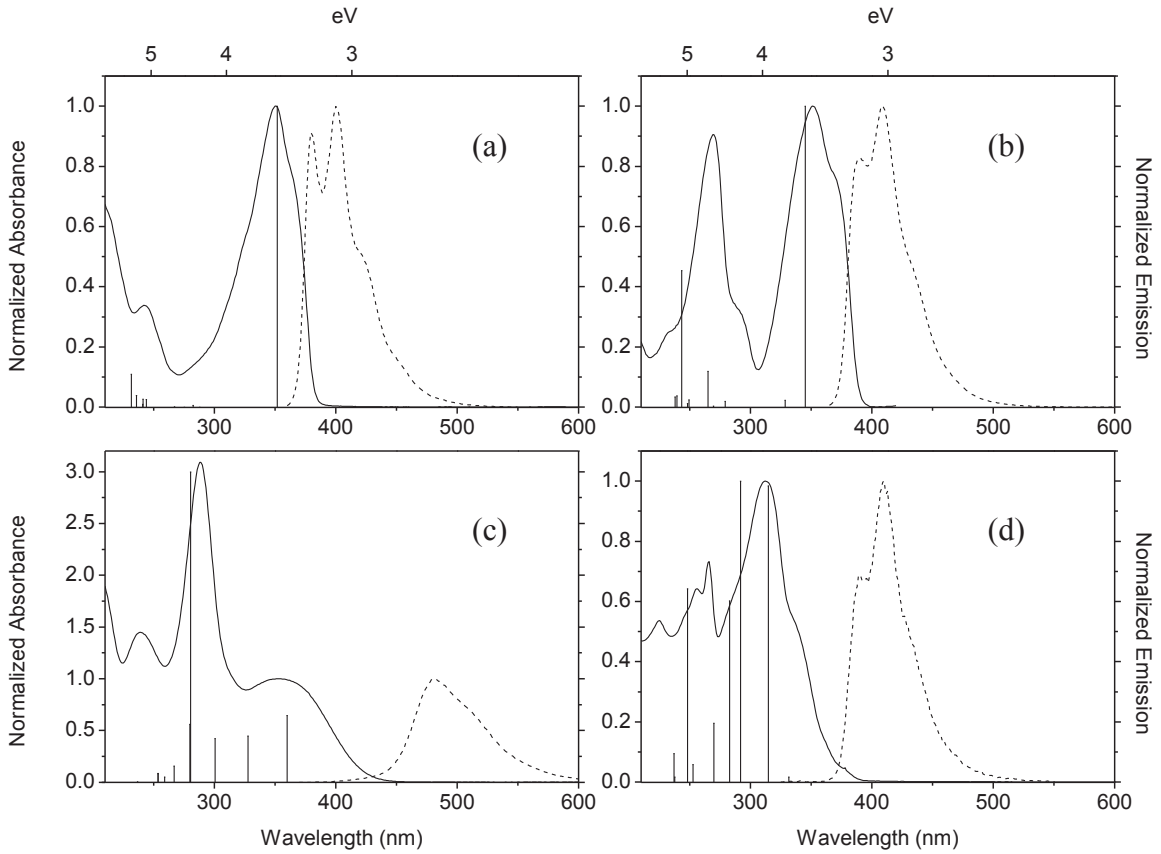
eV
5
4
3
(a)
(b)
(c)
(d)
Normalized Absorbance
Normalized Emission
Wavelength (nm)
300
400
500
600
0.0
0.2
0.4
0.6
0.8
1.0
0.5
1.5
2.0
2.5
3.0

Figure 4. Web version

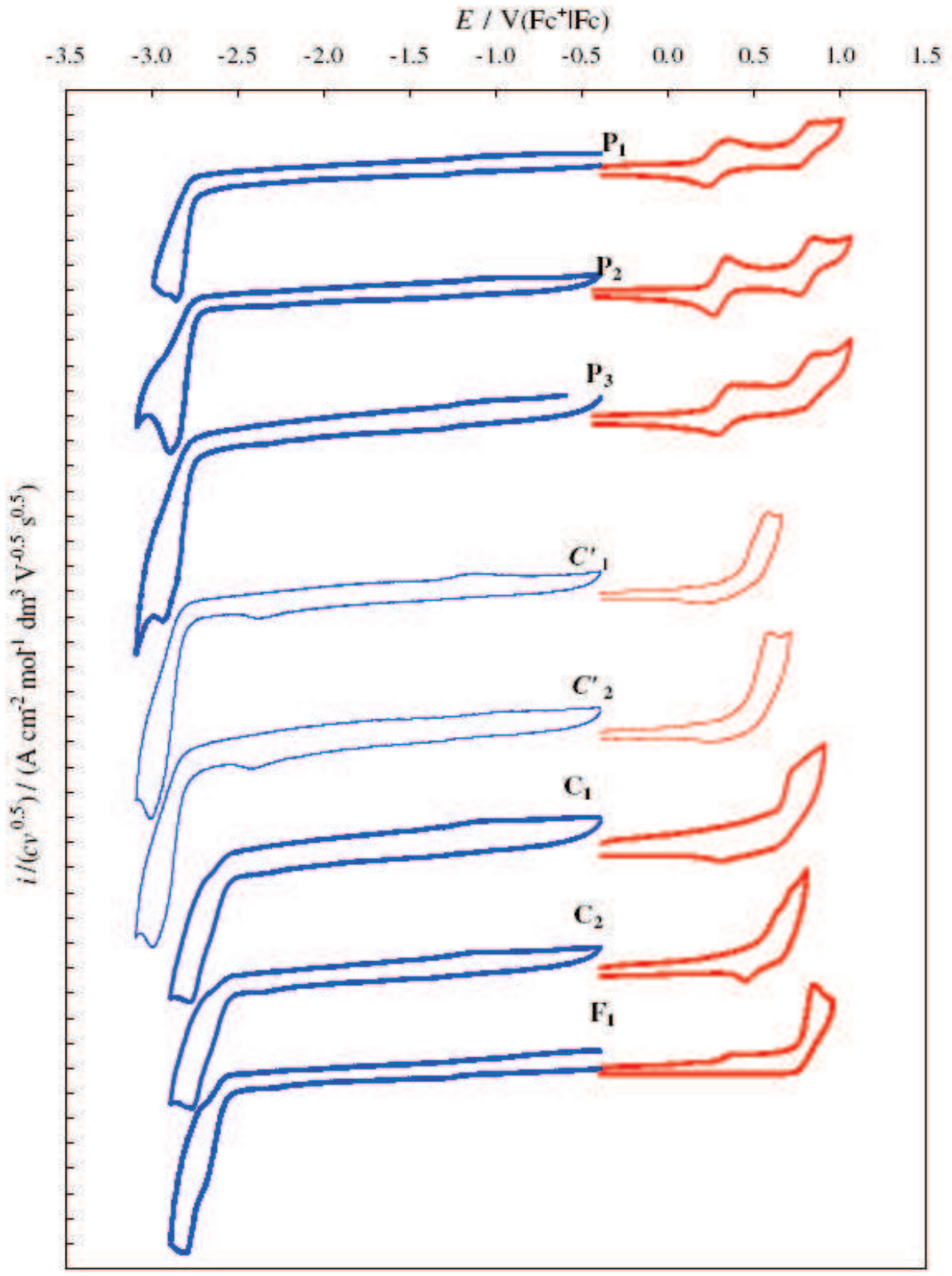

Figure 4. Print version

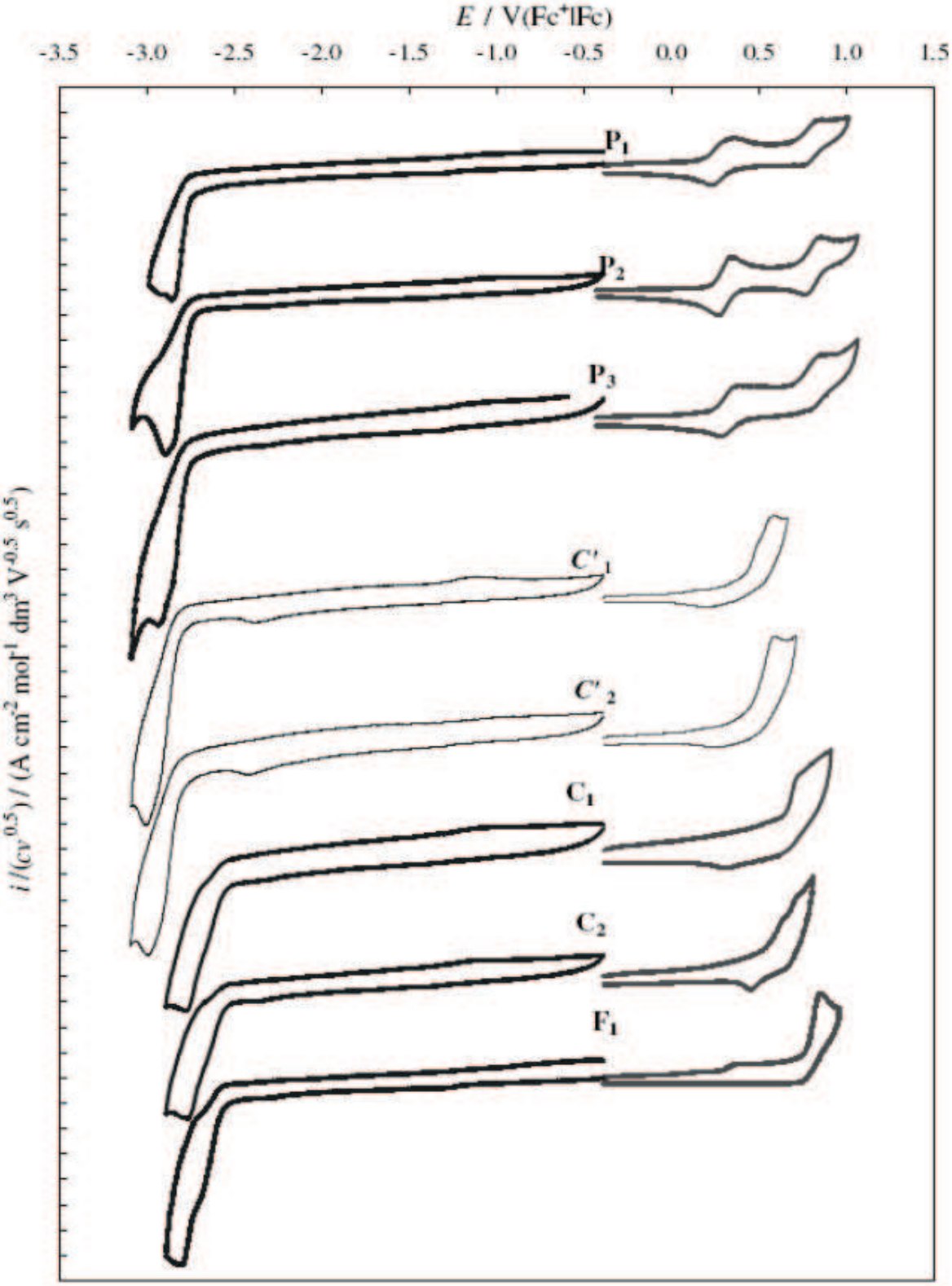

Figure 5. Web version

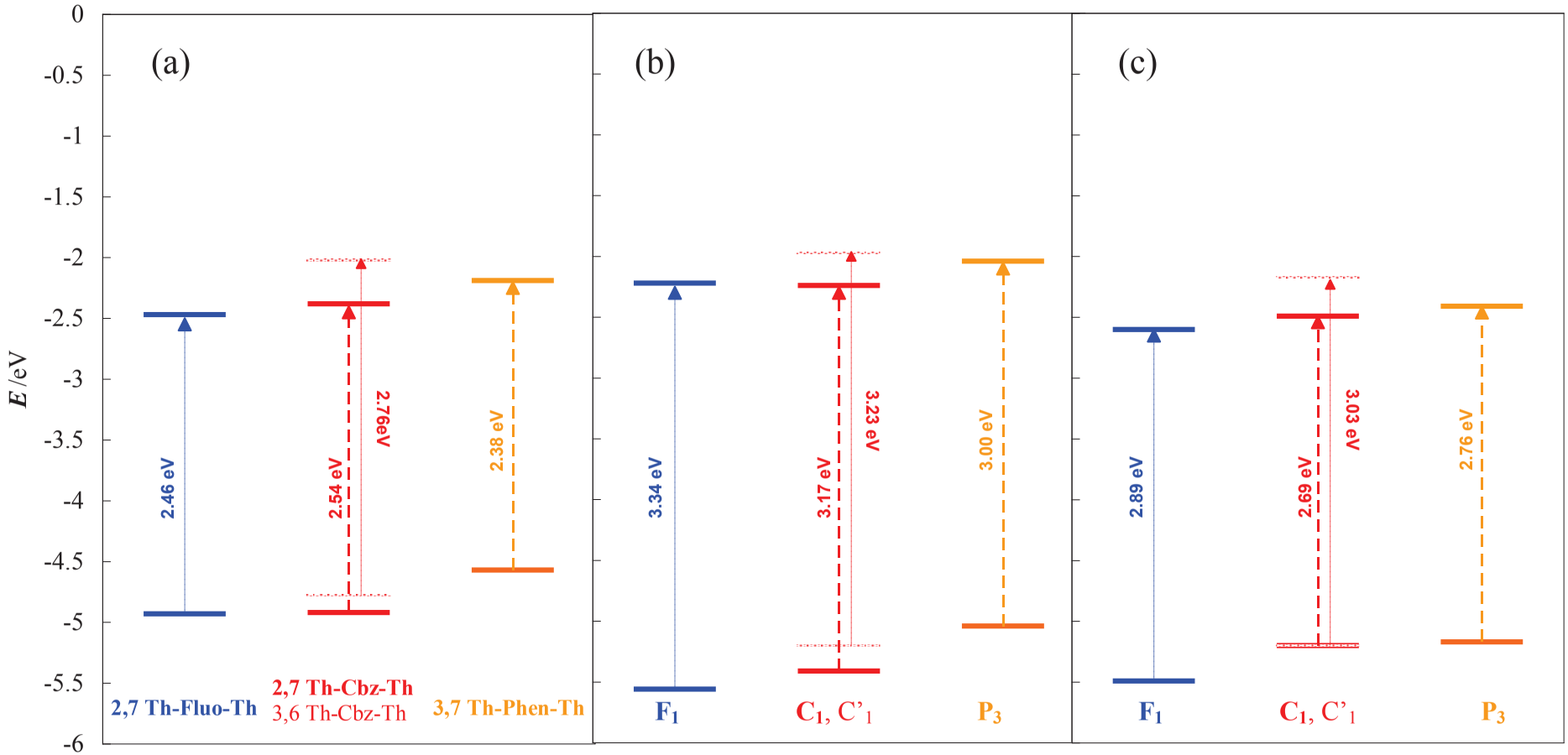

Figure 5. Print version

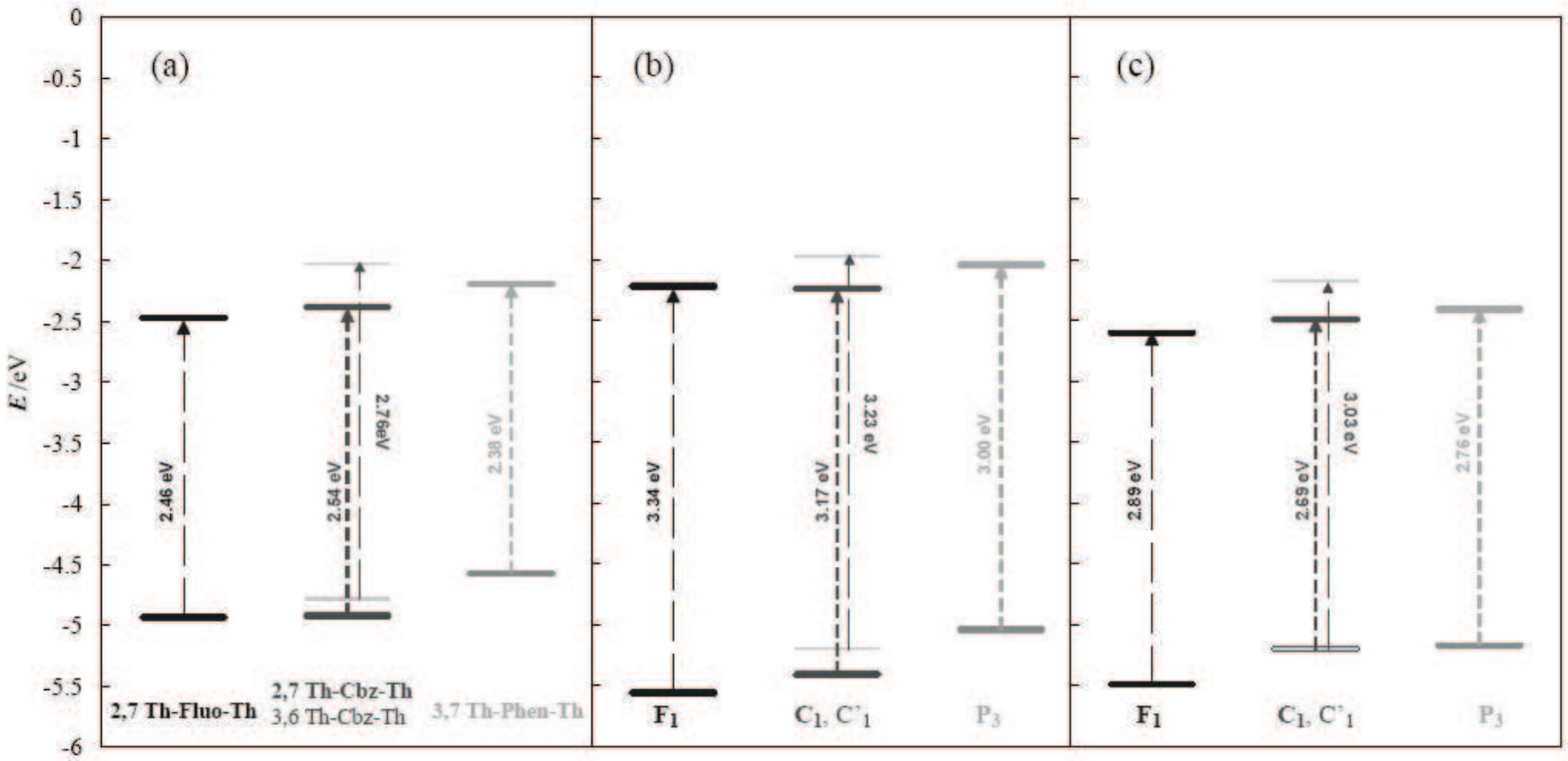

Figure 6. Web version

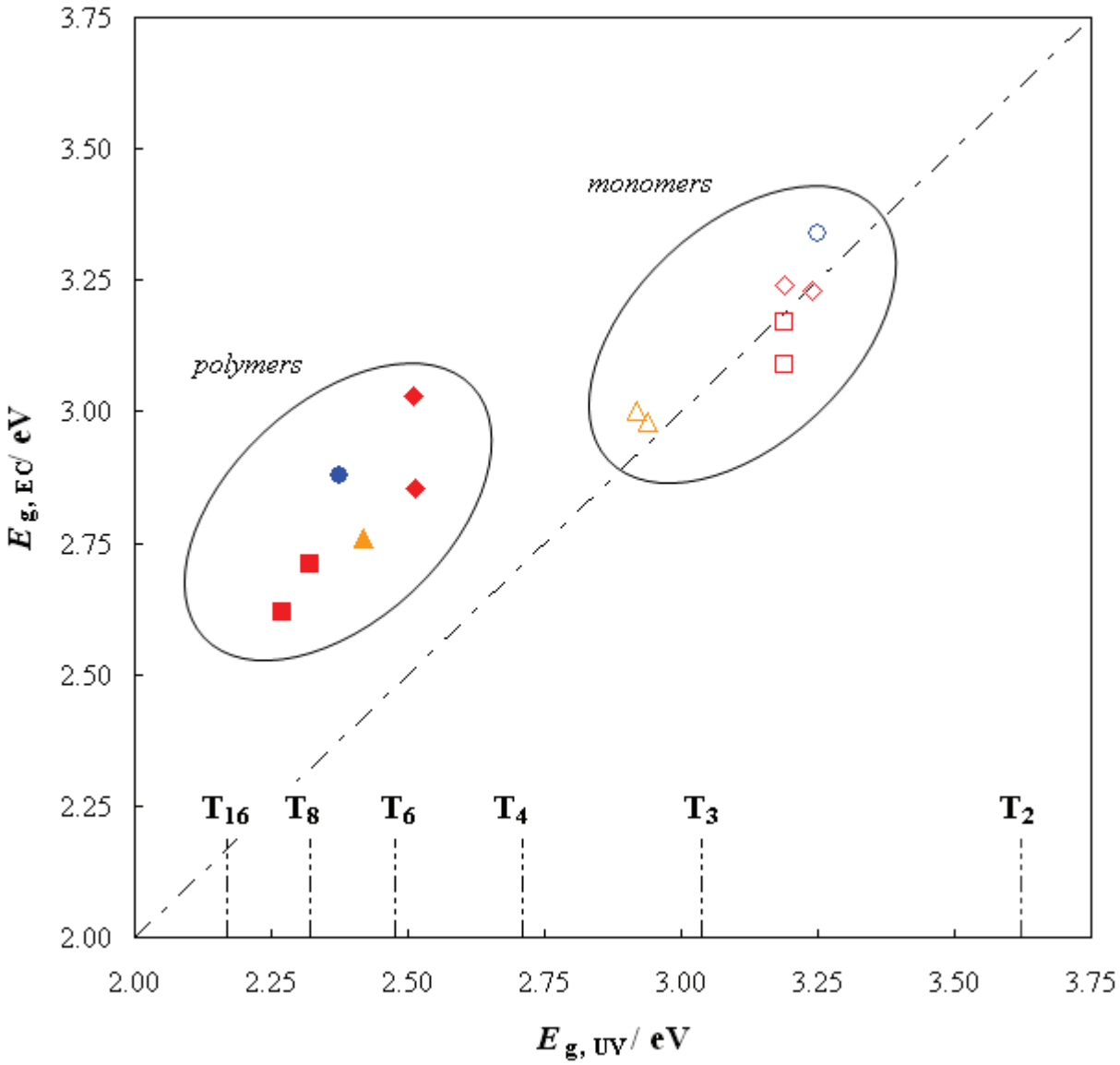

Figure 6. Print version

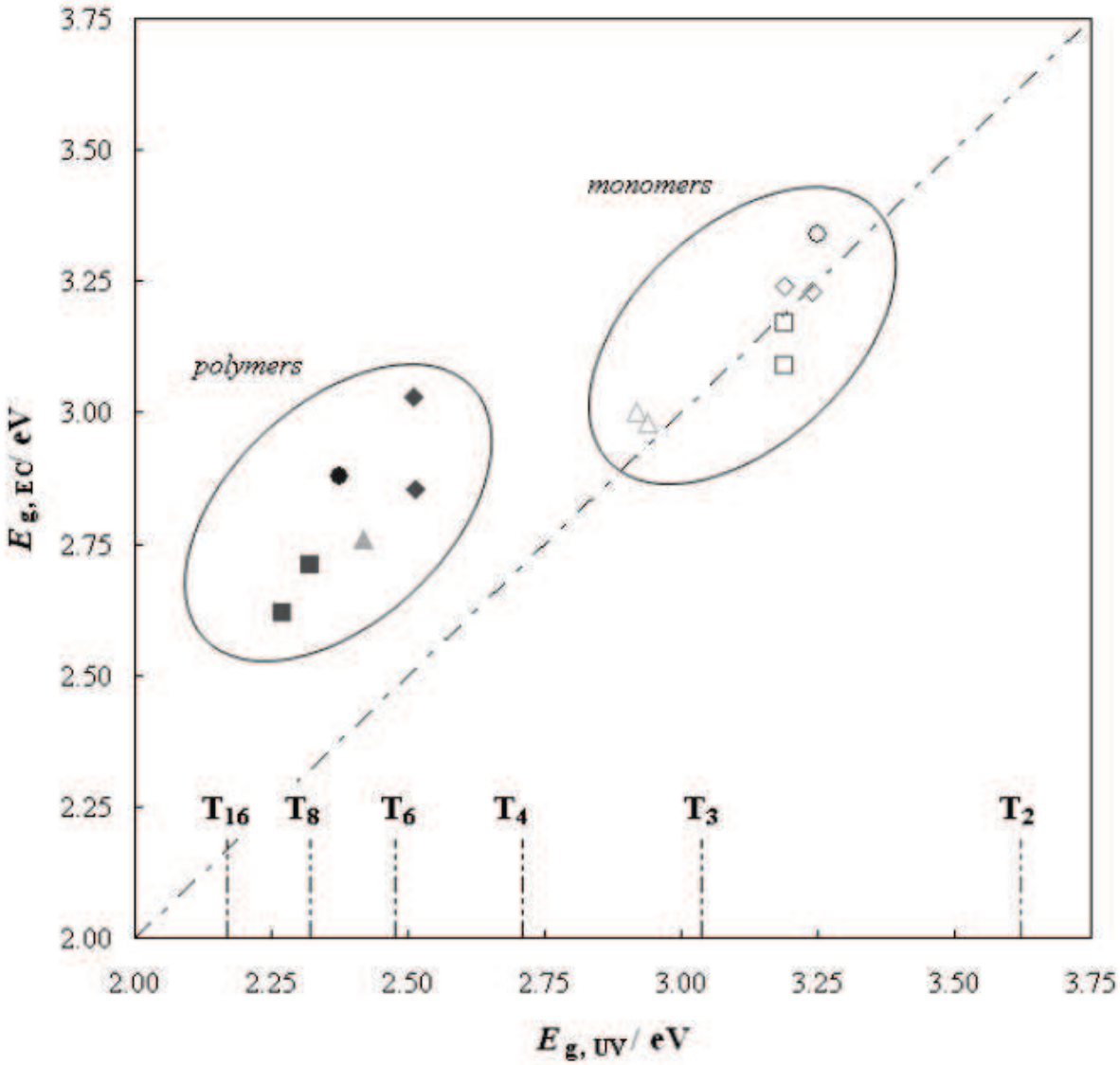

Figure 7. Web version

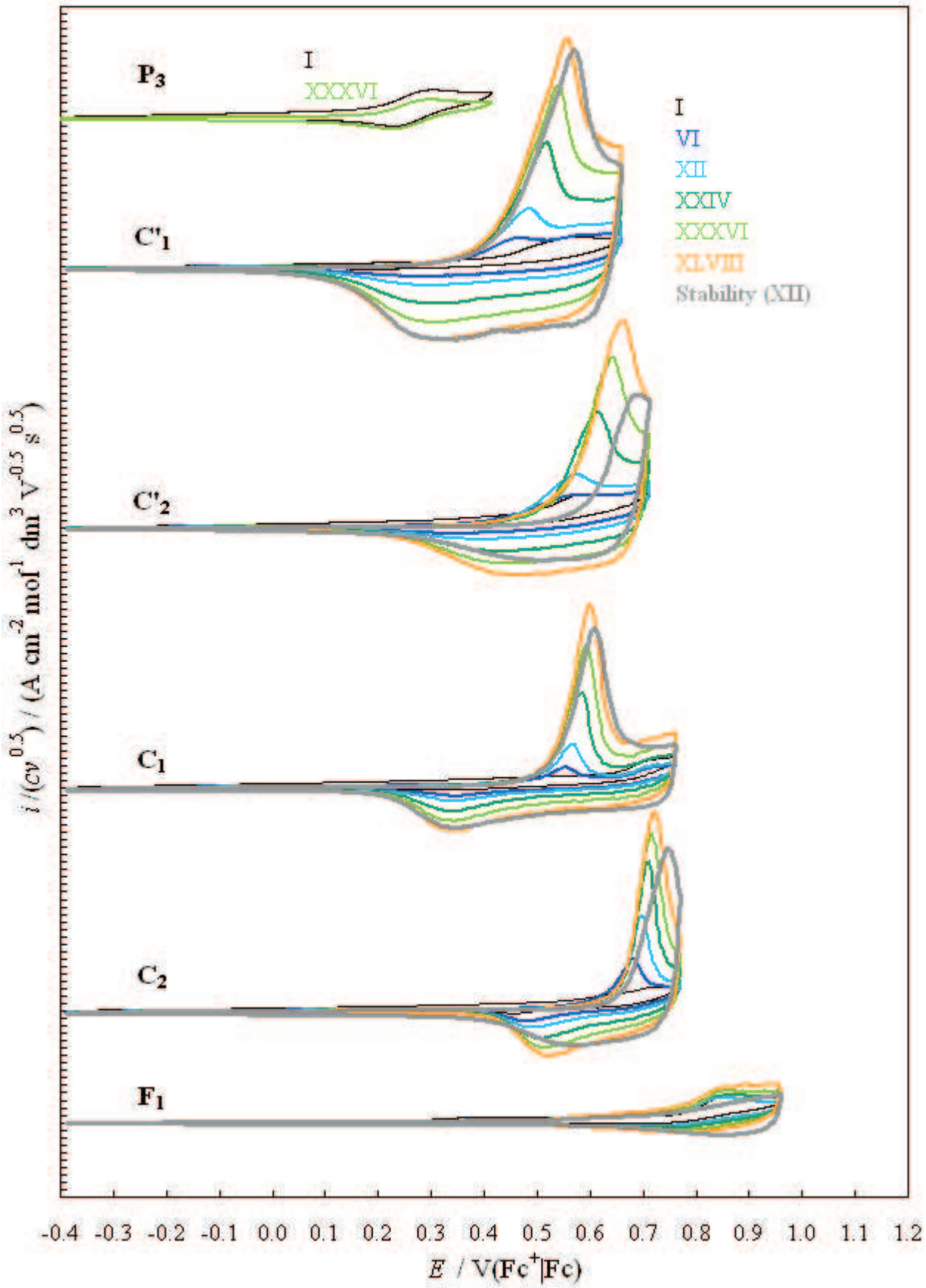

Figure 7. Print version

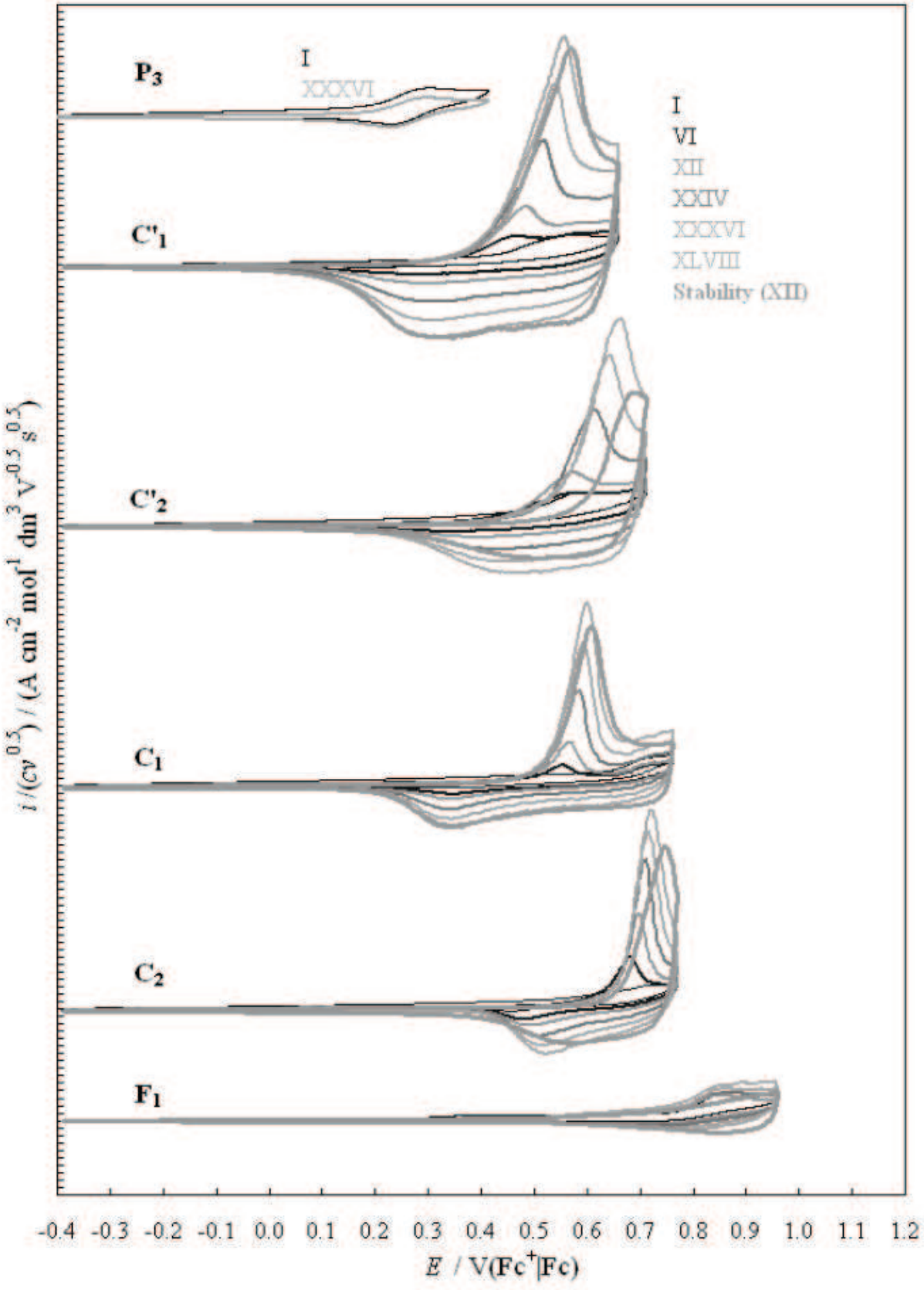

Figure 8. Web version

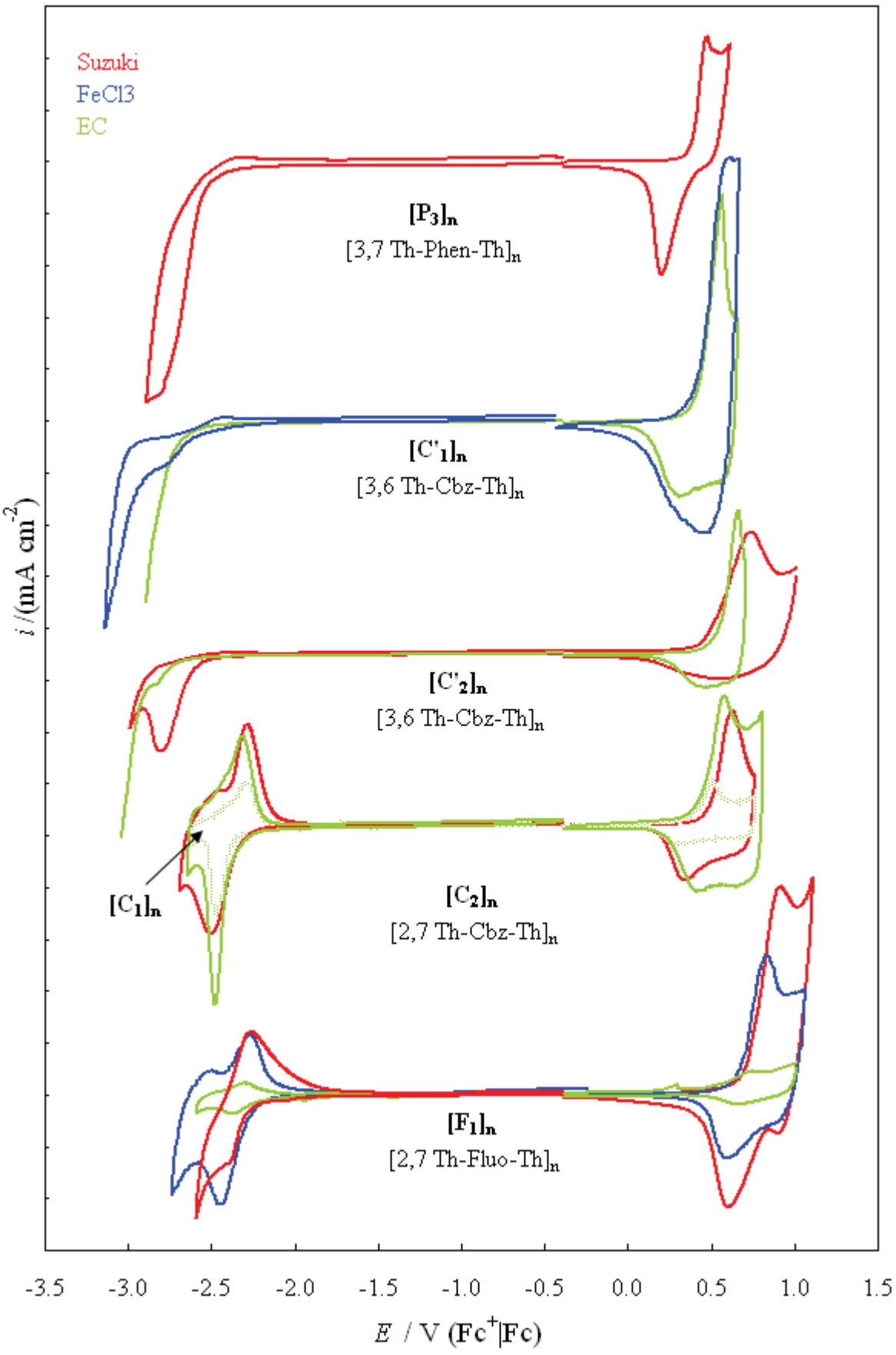

Figure 8. Print version

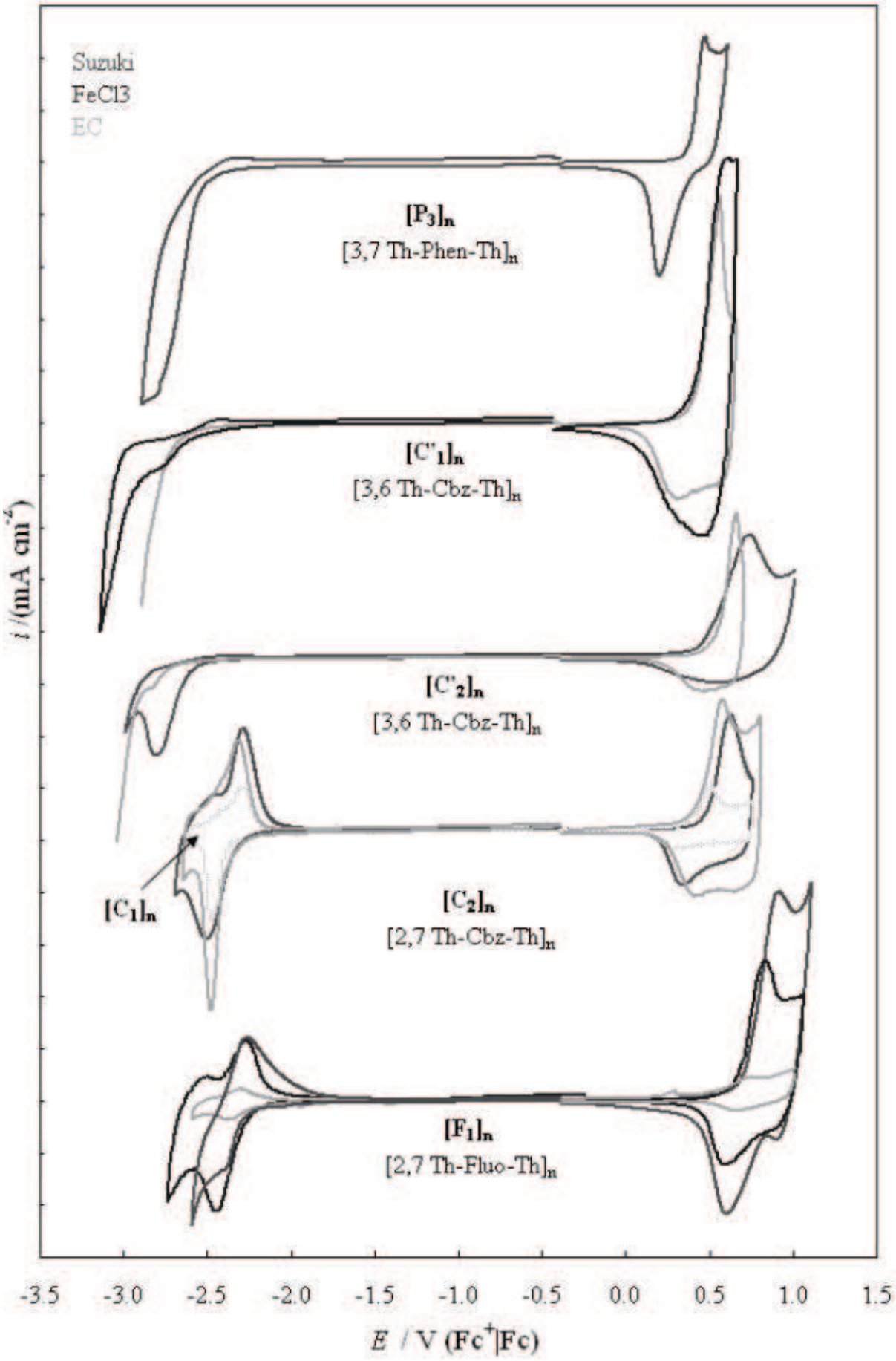

Figure 9.

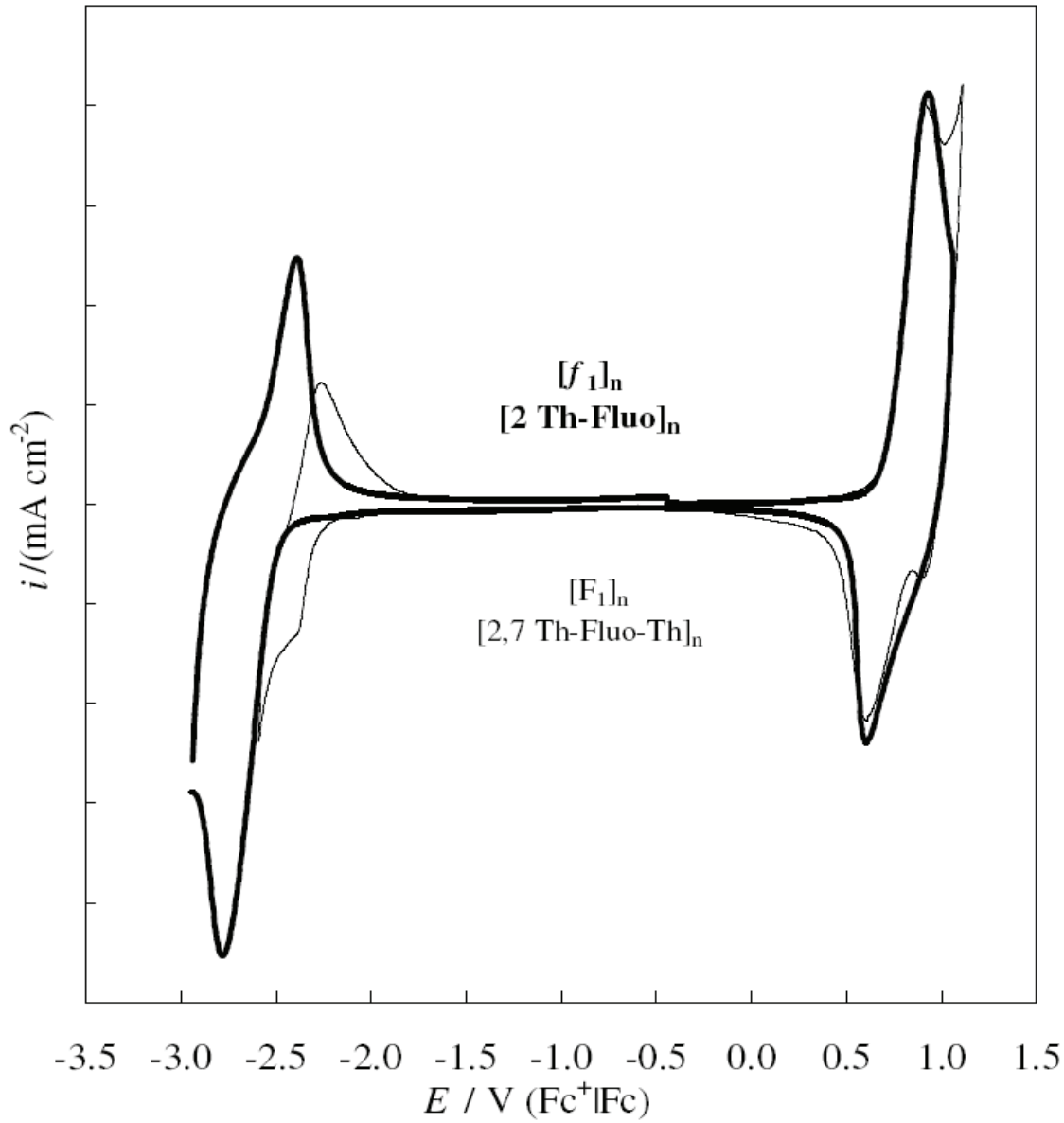
[f 1]n
[2 Th-Fluo]n
[F1]n
[2,7 Th-Fluo-Th]n
i /(mA cm-2)
-3.5 -3.0 -2.5 -2.0 -1.5 -1.0 -0.5 0.0 0.5 1.0 1.5
E / V (Fc+|Fc)

Figure 10. Web version

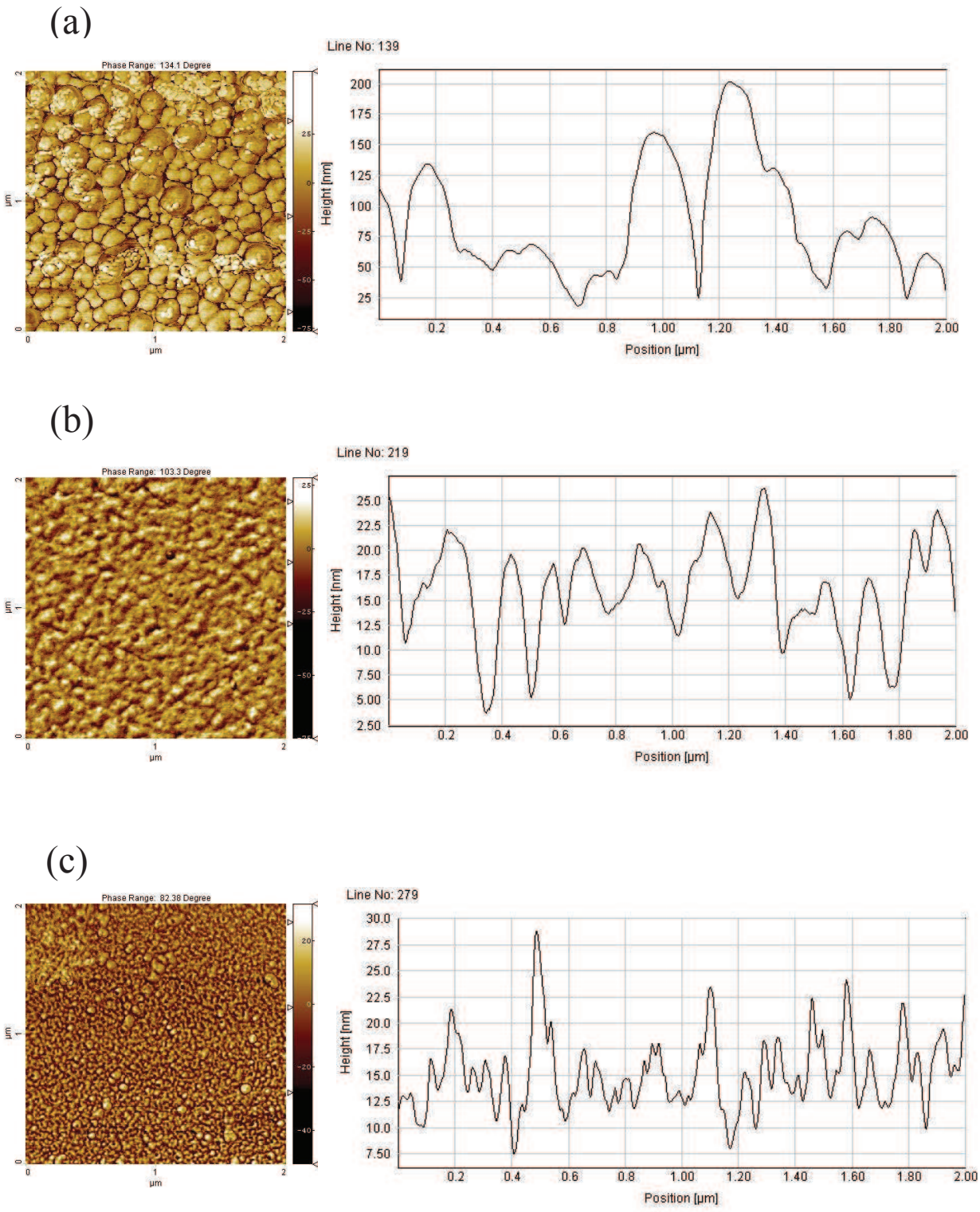

Figure 10. Print version

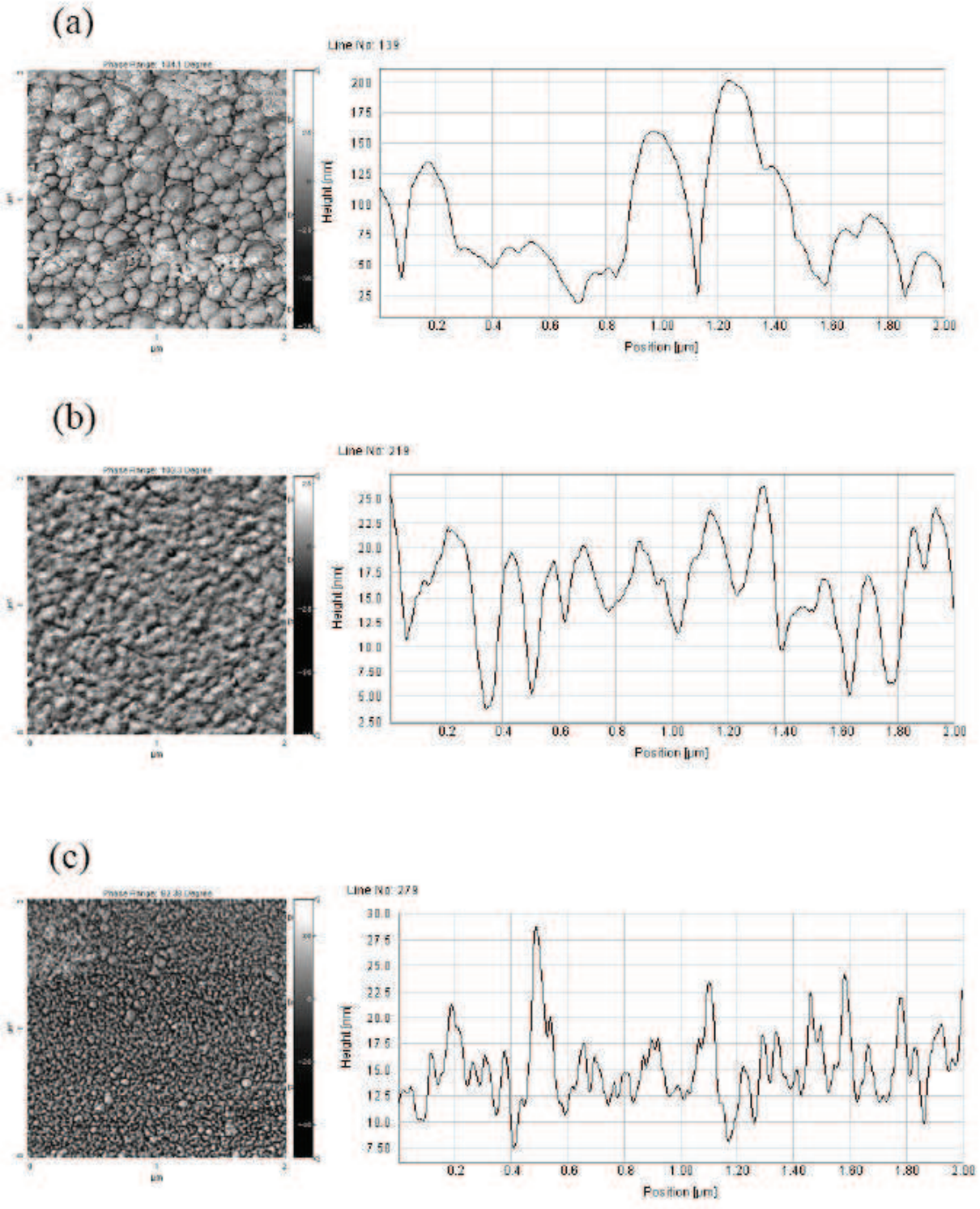

Supplementary Materials

Click here to download Supplementary Materials: Appendix A (Synthesis, details) Rev.doc

Supplementary Materials

Click here to download Supplementary Materials: Appendix B (Theoretical Computations, details) Rev.doc

Supplementary Materials

Click here to download Supplementary Materials: Appendix C.doc

***Research Highlights**

Effect of aromatic core on electronic properties in thiophene-X-thiophene trimers

The lower the electron richness of X core, the deeper the HOMO level

Different thiophene positions on X lead to kinked structure with lower conjugation

The fluorene structure exhibits the lowest Stokes shift and the highest quantum yield

The corresponding polymers obtained through three routes were studied.